North Carolina Agricultural and Technical State University
Aggie Digital Collections and Scholarship

Dissertations | Electronic Theses and Dissertations

2010

Effects Of Variable Friction Coefficient On The Pressure Distribution Between A Rolling Cylindrical Element And A Deformable Flat Surface

Francis Davis
North Carolina Agricultural and Technical State University

Follow this and additional works at: https://digital.library.ncat.edu/dissertations

Recommended Citation

Davis, Francis, "Effects Of Variable Friction Coefficient On The Pressure Distribution Between A Rolling Cylindrical Element And A Deformable Flat Surface" (2010). *Dissertations*. 4.
https://digital.library.ncat.edu/dissertations/4

This Dissertation is brought to you for free and open access by the Electronic Theses and Dissertations at Aggie Digital Collections and Scholarship. It has been accepted for inclusion in Dissertations by an authorized administrator of Aggie Digital Collections and Scholarship. For more information, please contact iyanna@ncat.edu.

EFFECTS OF VARIABLE FRICTION COEFFICIENT ON THE PRESSURE DISTRIBUTION BETWEEN A ROLLING CYLINDRICAL ELEMENT AND A DEFORMABLE FLAT SURFACE

by

Francis Davis

A dissertation submitted to the graduate faculty
in partial fulfillment of the requirements for the degree of
DOCTOR OF PHILOSOPHY

Department: Mechanical Engineering
Major: Mechanical Engineering
Major Professor: Dr. Samuel Owusu-Ofori

North Carolina A&T State University
Greensboro, North Carolina
2010

ABSTRACT

Davis, Francis. EFFECTS OF VARIABLE FRICTION COEFFICIENT ON THE PRESSURE DISTRIBUTION BETWEEN A ROLLING CYLINDRICAL ELEMENT AND A DEFORMABLE FLAT SURFACE. (**Major Advisor: Dr. Samuel P Owusu-Ofori**). North Carolina Agricultural and Technical State University.

The goal of this research is to develop a technique to accurately determine the characteristics of the pressure distribution during a rolling process. The determination of the accurate characteristics of a pressure distribution within the contact zone is essential to the accurate estimation of the energy and power requirements for the plastic deformation of the part. It has been determined by metal formers that the nature of the pressure distribution is very sensitive to the value of the coefficient of friction between the roller and the deformed part. It has also been determined that the physics of the deformation process points to a variable coefficient of friction between the roller and the part. However, current research and practices result in the use of a constant friction coefficient. This dissertation explores the development of a technique to determine a quantitative relationship between the variable friction coefficient and the process parameters.

This work considers the friction coefficient as a function of the roll angle and seeks to determine a quantitative relationship between them. The pressure distribution is then developed using a varying friction coefficient model. In this study, current insufficient research models are modified using a technique in which the contact region is analyzed in a piecewise manner from the entry to the exit points and the instantaneous

coefficient of friction extracted for each element. Consequently, the friction coefficient is determined as a function of the roll angle. The pressure distribution is then developed within the contact region using the instantaneous friction coefficient model. Results show that a "rule-of-thumb" method used by industry overestimates the pressure distribution. This results in the use of more power than needed for the operation. The current published methods, on the other hand, underestimate the pressure distribution. A cost-effective friction coefficient measuring technique has been developed and tested. An experiment was run on a laboratory rolling mill equipment using 1100 aluminum as the work material. The experimental results show that the friction coefficient varies within the contact region as expected. The results indicate that the power requirement developed from the proposed varying coefficient of friction model is 18% less than the power developed by using the industry method and about 8% less than the current published methods.

School of Graduate Studies
North Carolina Agricultural and Technical State University

This is to certify that the Doctoral Dissertation of

Francis Davis

has met the dissertation requirements of
North Carolina Agricultural and Technical State University

Greensboro, North Carolina
2010

Approved by:

Dr. Samuel P Owusu-Ofori
Major Advisor

Dr. DeRome Dunn
Committee Member

Dr. Frederick Ferguson
Committee Member

Dr. John Kizito
Committee Member

Dr. Mannur Sundaresan
Committee Member

Dr. Samuel P Owusu-Ofori
Department Chairperson

Dr. Alan Letton
Interim Associate Vice Chancellor
for Research and Graduate Dean

DEDICATION

To my Parents, Host Parents and Family: Emmanuel Davis Snr, Rev Elizabeth Davis, Dan and Helen Self, Esther Amoakohene Davis, Elizabeth Baaba Davis, and Emmanuel Kwamina Davis.

BIOGRAPHICAL SKETCH

Francis Davis was born on September 16th, 1968 at Cape Coast, Ghana. He received his Diploma in Mechanical Engineering in 1994, Bachelor of Science in Mechanical Engineering in 1998, and Master of Philosophy in Mechanical Engineering from Kwame Nkrumah University of Science and Technology, Ghana in 2004. He is currently a lecturer at Kwame Nkrumah University of Science and Technology. He is a candidate for the PhD. in Mechanical Engineering.

ACKNOWLEDGMENTS

My foremost acknowledgement is to God Almighty, through whose grace and power this work has been possible. God works through vessels and in this research, the vessel He (God) chose was Dr Samuel P Owusu-Ofori. Prof, thanks for the immense support and direction. I also express my appreciation to Drs, Frederick Ferguson, Mannur Sundaresan, John Kizito, and Derome Dunn for ably serving on my dissertation committee. I express thanks to Foreign Fulbright Student Program and KNUST for their support. Gratitude is also due Mr. Bruce Howe for machining parts of the rolling mill sensor used in the experimental work. Last, but not the least, I must express thanks to Dr. Ransford Baidoo, John Skujins, Oliver Lewis, Kwadwo Mensah Darkwa, Emmanuel Baisie, Ruben Kotoka, Richard Opoku, Joseph Acheampong, and the entire Mechanical Engineering Department staff for all the diverse support that I received from them in the course of my studies.

TABLE OF CONTENTS

LIST OF FIGURES

FIGURES **PAGE**

LIST OF TABLES

TABLES **PAGE**

LIST OF SYMBOLS

h_0	Initial Slab Thickness
h_f	Final Slab Thickness
V_0	Entry Velocity
V_f	Exit Velocity
R_0	Roll Radius
N	Rotational Speed
V_r	Roll Velocity
$d\theta$	Change in Roll Angle
θ	Roll Angle
F	Friction Force
P	Normal Pressure
σ	Normal Stress
τ	Shear Stress
μ	Friction Coefficient
$\acute{\varepsilon}$	Strain Rate
F_{app}	Applied Force
F_{net}	Net Force
μ_s	Static Friction Coefficient
μ_k	Kinetic Friction Coefficient
E_T	Total Dissipation Energy
E_F	Energy in Overcoming Friction

E_D	Energy in Overcoming Discontinuities
E_P	Plastic Deformation Energy
m	Shear Factor
K	Shear Yield Strength
P_r	Roll Separation Force
$\bar{\sigma}$	Average Flow Stress
R'	Radius of Flattened Roll
r	Reduction
σ_y	Yield Strength
σ_{xb}	Back Tension
σ_{xf}	Front Tension

LIST OF ABBREVIATIONS

FEM	Finite Element Method
DEFEL	Finite-Element Hydrodynamic Computer Code
MATLAB	Matrix Laboratory
AMATROL	Metal Processing Center Rolling Mill Equipment
MATROL	Rolling Matlab Computer Program
UBM	Upper Bound Method
MM	Micro Measurement
SGRoll	Strain Gaged Roll
S5000S	System 5000 Scanner
SSS	Smart Strain Software
FWD	Forward

CHAPTER 1

INTRODUCTION

The contact region between a rolling cylindrical element and a flat surface can lead to elastic or plastic deformation depending on the contact pressure. Some of the forms of elastic deformation are an automobile tire on the road, a railroad wheel, and a rolling bearing. Plastic contacts in rolling include a pin on a dough, a rolling stone on a pavement under construction, and rolling mills. This chapter gives the background of the research work and how the dissertation is organized. The motivation of the research and its significance are also presented.

1.1 Background

In order to analyze the stress between the rolling cylindrical elements and the flat surfaces, rolling contact models are needed. Figures 1.1 and 1.2 illustrate physical models for rolling contact applications. Figure 1.1 shows a rolling cylindrical element on a flat surface where the surfaces in contact deform elastically. Contact model A in Figure 1.2(a) shows a rolling cylindrical element on a stationary flat surface where the flat surface deforms plastically. The contact model B in Figure 1.2(b) shows a rolling cylindrical element on a moving flat surface where the flat surface undergoes plastic deformation.

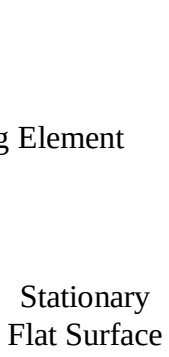

Figure 1.1. Elastic Contact Model

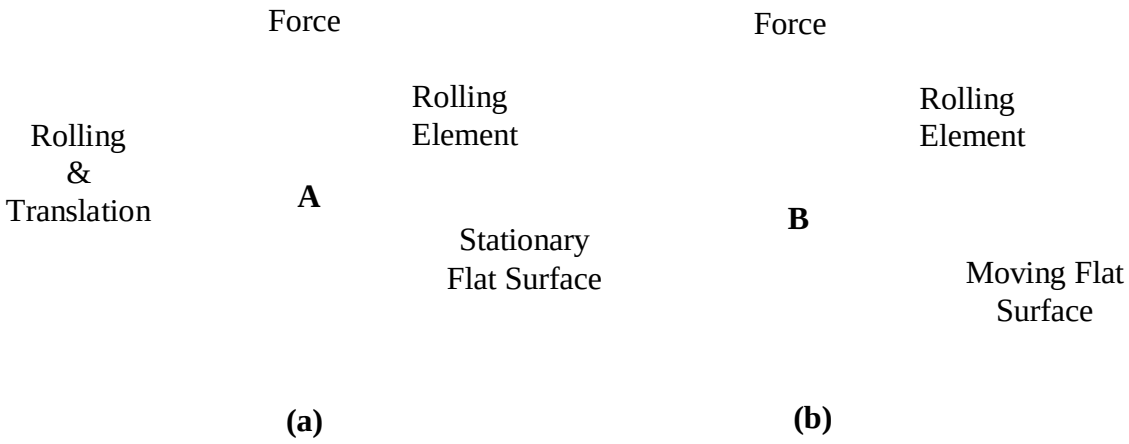

Figure 1.2. Plastic Contact Models: (a) Stationary Flat Surface (b) Moving Flat Surface

This work is interested in the contact model B as in Figure 1.2(b) because of its direct application in metal deformation processes. A typical application in manufacturing is slab rolling operation. Figure 1.3 illustrates an example of slab rolling in which a metal slab is squeezed continuously through two identical rolls rotating in opposite directions. In a slab rolling process, the friction force within the contact region is necessary for the transmission of deformation energy from the rolls to the part.

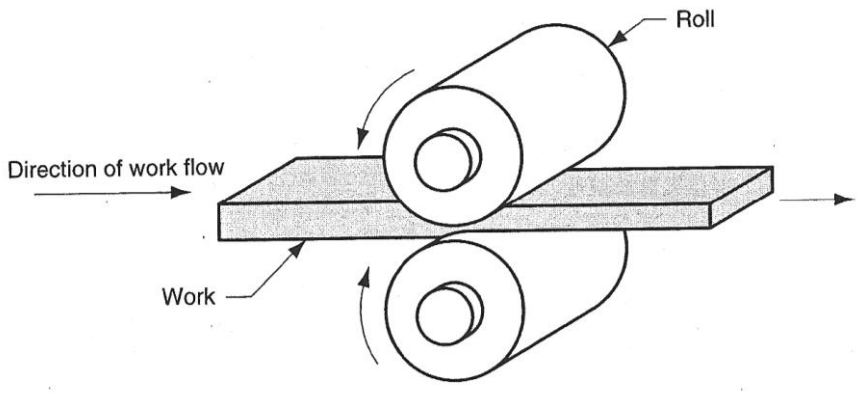

Figure 1.3. Slab Rolling Operation

The compressive force, which is responsible for the change in thickness of the part, includes a friction component. The knowledge of the effect of the coefficient of friction is critical in the evaluation of the power requirements for the rolling operation [Jiang, 2004], [Jiang, 2003], [Larkiolda, 1996], [Keife, 1994]. This research focuses on predicting the instantaneous friction coefficient between a rolling cylindrical element and a flat surface. Results obtained from the research could be used for a more accurate evaluation of the power and energy requirements.

1.2 Motivation of Research

Figure 1.4 shows a model for plastic contact rolling. In this figure, h_0 is the initial slab thickness, h_f is the final slab thickness, V_0 is the entry velocity, V_f is the exit velocity, R_0 is the roll radius, N is the rotational speed of the roll, V_r is the roll velocity, and $d\theta$ is the included roll angle for the elemental strip within the deformation zone.

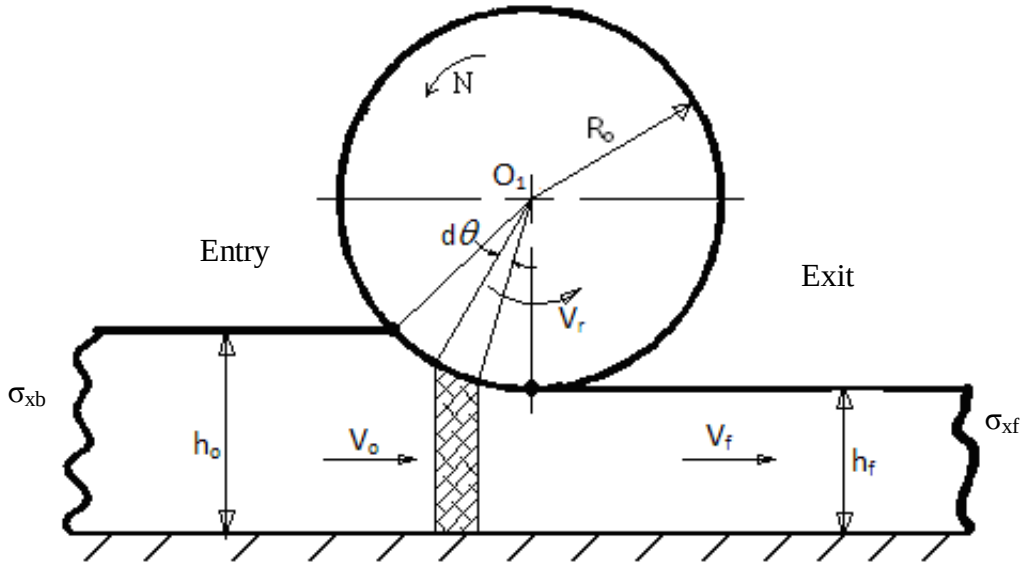

Figure 1.4. Plastic Rolling Contact Model

From Figure 1.4, a force analysis on an elemental strip within the contact region results in a stress equation shown in Equation 1.1. See Appendix A for the derivation of Equation 1.1. In this equation, σ_x is the axial stress, P_θ is the roll pressure at angle θ, and

$$\frac{\partial(\sigma_x h)}{\partial\theta} = P_\theta R\left(\sin\theta(1+\mu_\theta) \pm \cos\theta\left(\mu_\theta + \mu_\theta^2\right)\right) \tag{1.1}$$

μ_θ is the friction coefficient. The stress equation shows a high influence of the frictional coefficient. To reduce the effects of friction, a second roller could be introduced as shown in Figure 1.5. Once again, a force analysis on an elemental strip within the contact region results in a stress equation shown in Equation 1.2. It can be seen from Equation 1.2 that the influence of friction has been greatly reduced with the loss of the second term in Equation 1.1. Equation 1.2 was first derived by Von Karman [Dieter, 1976].

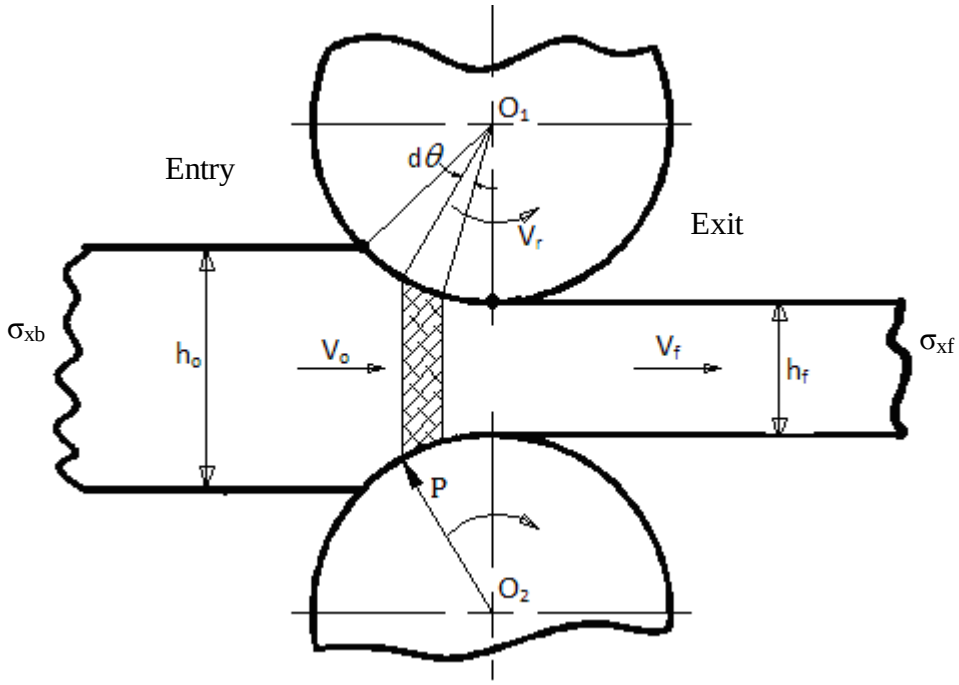

Figure 1.5. Double Roller Plastic Rolling Contact Model

$$\frac{\partial(\sigma_x h)}{\partial\theta} = 2P_\theta R(\sin\theta \pm \mu_\theta \cos\theta) \tag{1.2}$$

According to the principles of physics, the magnitude of the friction force between surfaces in contact decreases continuously as the part transitions from the quasi-static to the dynamic modes. The physical behavior of the friction force is illustrated in Figure 1.6. In relation to dynamic rolling contact, the friction force between surfaces in contact changes from the part entry point to the exit point. As a result, the friction coefficient should also vary.

Researchers in this field have solved the stress equation with several assumptions. One of the assumptions is that the friction coefficient is constant within the contact region.

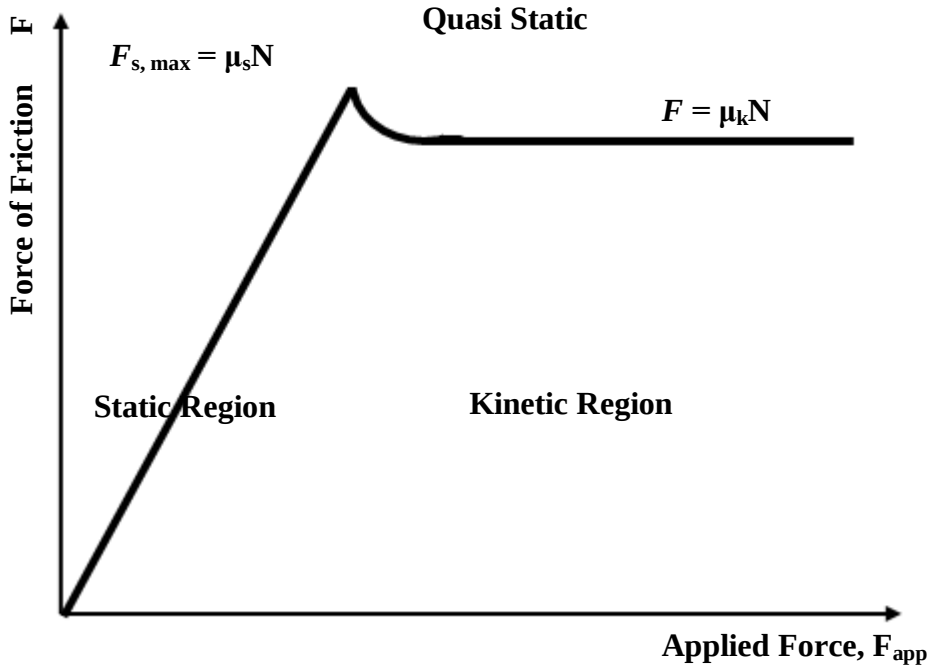

Figure 1.6. Friction Coefficient Curve

The relationship between the normal pressure P and the horizontal compressive stress σ_x in Equation 1.2 is given by considering the distortion energy criterion of yielding for the plane strain condition. This is expressed in Equation 1.3.

$$\sigma_1 - \sigma_3 = \frac{2}{\sqrt{3}}\sigma_y = 2K = \sigma_0 \tag{1.3}$$

where σ_1 and σ_3 are the principal stresses within the contact zone, and σ_y, σ_0, and K are the yield strength, flow stress, and the shear yield strength of the work material, respectively.

Considering a stress element within the deformation zone as shown in Figure 1.7 and assuming that the frictional force is very small and can be neglected, the principal stresses in the element can be evaluated as $\sigma_1 = \sigma_x$ and $\sigma_3 = -P$.

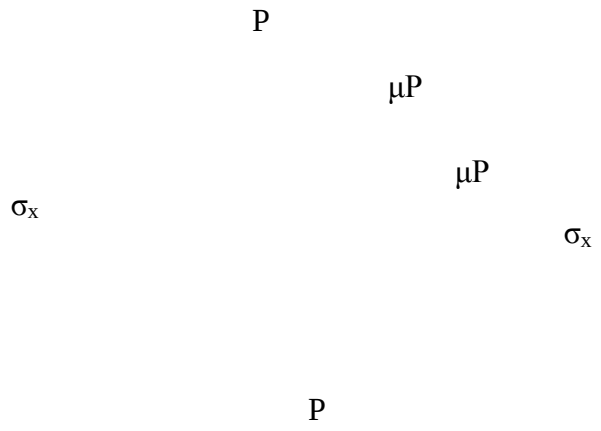

Figure 1.7. Stress Element in Deformation Zone

The negative sign accounts for the compressive nature of the stress. Thus, Equation 1.3 can be written in terms of σ_x and P as shown in Equation 1.4.

$$\sigma_x + P = 2K \tag{1.4}$$

Now, eliminating σ_x from Equations 1.2 and 1.4 and noting that the friction force changes direction in accordance with the relative speed between the roller and the part results in Equation 1.5. The complexity of Equation 1.5 makes it necessary to obtain solutions by numerical methods. Some simplification has been suggested by other researchers for the purpose of obtaining a closed-loop solution to Equation 1.5.

$$\frac{\partial\left[(2K-P)h\right]}{\partial\theta} = 2PR\left(\sin\theta \pm \mu\cos\theta\right) \tag{1.5}$$

The simplifications are that: (1) the coefficient of friction (μ) is constant at all points on the arc of contact, (2) the angle θ subtended by the work in the deformation zone is very small, (3) the shear yield strength (K) is constant, and (4) there is an identifiable point where no slip occurs between roller and the part, known as the neutral point. Applying

the above simplifications to Equation 1.5 and integrating, results in Equations 1.6, 1.7, and 1.8. For details of the integration refer to [Gosh, 1986].

$$\left(\frac{P}{2K}\right)_{Before\ Neutral\ Point} = \frac{h}{h_0}\left(1-\frac{\sigma_{xb}}{2K}\right)e^{\mu(\lambda_0-\lambda)} \tag{1.6}$$

$$\left(\frac{P}{2K}\right)_{After\ Neutral\ Point} = \frac{h}{h_f}\left(1-\frac{\sigma_{xf}}{2K}\right)e^{\mu\lambda} \tag{1.7}$$

$$\lambda = 2\sqrt{\frac{R}{h_f}}\tan^{-1}\left(\sqrt{\frac{R}{h_f}}\,\theta\right) \tag{1.8}$$

where, h_0 and h_f represent entry and exit thickness of the deformed part, respectively,. $\frac{P}{2K}$ represent a non-dimensional roll pressure, σ_{xb} and σ_{xf} represent back and front tensions, respectively. The pressure at the neutral point is determined from either Equation 1.6 or 1.7. The value of the parameter λ corresponding to the neutral point (λ_n) is obtained by equating Equations 1.6 and 1.7. The result is shown in Equation 1.9.

$$\lambda_n = \frac{1}{2}\left[\frac{1}{\mu}\ln\left\{\frac{h_f}{h_0}\left(\frac{1-\sigma_{x0}/2K}{1-\sigma_{xf}/2K}\right)\right\}+\lambda_0\right] \tag{1.9}$$

The location of the neutral point θ_n corresponding to λ_n can be obtained from Equation 1.8. In practice, the estimation of pressure distribution assuming constant friction coefficient has been found to be deficient and results in gross over estimation of the rolling stresses. This leads to inconsistencies in product performance.

Several other researchers have recognized the need to develop methods which lead to a better estimation of the coefficient of friction. These authors derived the friction coefficient models within the contact region for a cold rolling process in terms of geometrical parameters and material properties. However a careful analysis of their results still leads to the assumption that the friction coefficient is constant within the contact region. Their works, though, yielded a more accurate constant friction coefficient than the ones used by the industry through trial and error.

The assumption of a constant coefficient of friction is unrealistic because there is a relative motion between the surface of the part and the rolls which causes sliding, sticking and slipping actions within the contact region. Since the work flow is continuous, there is a gradual change in the relative speed between the rolls and the part. However, there is a point at which the roll and the part speeds are equal. This point is known as the "no slip" point or the "neutral point". From the entrance of the roll to the "no slip" point, the roll moves faster than the work, while the work moves faster than the roll from the "no slip" point to the exit point. The above phenomenon reflects a varying friction coefficient within the contact region and not a constant friction coefficient as other researchers have alluded to.

This research seeks to provide a realistic estimation of instantaneous friction coefficient within the contact region for slab rolling operation. This dissertation seeks to quantify the friction coefficient within the contact region of a rolling cylindrical element on a flat surface as a function of the roll angle (θ).

1.3 Goals and Objectives

The goal of this research is to improve the accuracy in the estimation of force and pressure distribution within the contact region of a rolling cylindrical element on a flat surface. The specific objectives are:

1. To determine a quantitative relationship between the friction coefficient (μ) and the roll angle (θ),
2. To develop the pressure distribution within the contact region, assuming a varying friction coefficient from the entry to the exit point and to compare the results with existing models,
3. To study the effect of strain hardening on the pressure distribution within the contact region, and
4. To propose and demonstrate a technique to measure the coefficient of friction between a rotating roller and a flat surface under plastic deformation.

1.4 Significance of Study

In order to meet the ever-increasing demand for high quality and low cost products, it is very important to obtain accurate models for the evaluation of process parameters. Since the output of the cold rolling process is almost a finished product, controlling the parameters affecting this process is important. Engineers have to juggle a gamut of parameters such as the speed of deformation, the amount of deformation, the temperature at deformation, lubrication, and material properties in order to achieve a desired outcome. Among these parameters, an accurate prediction of the friction

coefficient within the contact region is a major challenge. The current methods used in the estimation of the friction coefficient within the contact region include experience, rule of thumb, trial and error, and use of empirical formulae. All of these assume that the friction coefficient is constant within the contact region. However, an accurate estimation of the friction coefficient must lead to a variable value within the contact region.

In this study, a quantitative relationship between the friction coefficient and process parameters replaces the current method of estimating the friction coefficient. The friction coefficient model would then be substituted into the stress equation, and the resulting differential equation would be solved to obtain a more accurate pressure and force distribution within the contact region than the current prediction models.

1.5 Organization of Report

This dissertation is organized into five chapters. The introduction, consisting of the background, objective, and significance of the study are presented in Chapter 1. Chapter 2 contains the literature review, which includes modeling methods used in contact rolling, rolling theories, review of scientific work done, review of friction coefficient models, friction measurement, and the pressure distribution. Chapter 3 involves the methodology of the research work. The proposed friction coefficient modeling technique and the demonstration of a friction coefficient measuring technique are treated in Chapter 3. The data analysis, results and discussions are presented in

Chapter 4. Chapter 5 closes the dissertation with the conclusions and recommendations for future work.

CHAPTER 2

LITERATURE REVIEW

Common engineering raw materials such as bars, plates, sheets, and strips are commonly produced by cold rolling. Cold-rolled sheets and strips constitute important parts of the total steel production and are among the major raw materials for the consumer goods industries such as, household appliances. Metals may be cold rolled to improve the physical properties, produce good surface finish, impart textured surfaces, dimensional control, and improve machinability. This chapter reviews the rolling theory, various modeling techniques, and scientific contributions of various researchers in the modeling techniques.

2.1 Slab Rolling Operation

Cold rolling in addition to production of raw materials is a practical method of imparting hardness to a material. Cold rolled sheets and strips are classified commercially as skin-rolled, quarter-rolled, half-hard, and full-hard to signify the amounts of reduction [Doyle, 1985]. Cold rolling produces uniform thicknesses and close tolerances in sheets, strips, and bars. Machinability of most steels is improved by cold working and for that reason cold rolled or drawn stocks are widely used in machining operations. Most cold rolling operations are done with small rolls in four high or cluster mills and tension is frequently applied at either end or both ends of the sheet to mitigate the adverse effects of the high pressures needed for the deformation process.

2.2 Modeling Techniques

There are three main modeling techniques in the rolling operation. These are: (1) the finite element method (FEM), (2) the energy or upper bound method, and (3) the slab method. Many researchers, including [Liu, 2007], [Gao, 2002], [Jeswiet, 1995], [Le, 2001], [Yuen, 1996], have modeled the rolling process using the Finite-Element Method. The Finite-Element modeling method uses a variational approach to formulate a function which consists of specific constitutive relations [Kopayashi, 1982]. The model was created as follows: The deformed body was divided into finite elements interconnected at nodal points. A function was expressed locally within each element in terms of the nodal point values associated with the particular element. The local element equations were then assembled into a generalized problem, which resulted in stiffness equations. The stiffness equations were assembled into a global matrix and solved for the nodal point values. Lau [Lau et'al, 1987] simulated high speed rolling of work hardening aluminum billet using a technique dubbed "Finite-Element Hydrodynamic Computer Code (DEFEL)". The billet was 1.25 inches in length and 0.625 inches in half-height. The area reduction was 20%, a roll radius of 2 inches, a tangential roll speed of 1200 in/s and the initial speed of billet was 900 in/s. The billet was modeled as an elastic-plastic material with work hardening. They used quadrilaterals formed by four crossed triangles as the elements. A total of 800 triangular elements with 431 nodes were used. The roll was modeled with 180 elements and 181 nodes. These FEM models gave accurate results. However, the computational times were very long and required mainframe computers, thus making it impractical for use in the control of the rolling mill.

The energy or upper-bound method predicts the maximum load and the deformation energy values and gives detailed information on the material flow. Lahoti modeled the rolling process using the upper bound method [Lahoti, 1979]. Hill's [Hill, 1963] kinematic admissible velocity field was used to derive expressions for the strain-rate components $\dot{\varepsilon}_x$, $\dot{\varepsilon}_y$, $\dot{\varepsilon}_z$, and the effective strain rate, $\dot{\varepsilon}$. The strain rate, flow stress (σ), and shear stress (τ) were used to calculate the total energy dissipation rate (E_T), given by the relation $E_T = E_P + E_F + E_D$. Where, E_P, E_F, and E_D, are energy rates due to plastic deformation, energy rate in overcoming friction, and energy rate due to shearing along the boundaries of velocity discontinuities. The total energy dissipation rate E_T was then minimized to obtain the values of the process parameters. According to Lahoti the upper-bound method and the velocity fields provided detailed information on the metal flow, but did not yield a specific roll-separating force.

The strip method, also known as the slab method, predicts the pressure distribution by analyzing the forces acting on elemental strip or slab in the deformation zone and integrating over the entire contact region. Figure 2.1 shows a finite number of strips within the deformation zone. Advantages of using the strip method include the following: (i) the computational time is shorter than that of the FEM method; (ii) the reduced computational time could enable an on-line control of the rolling mills; (iii) the analysis can be run on a personal computer rather than a mainframe; and (iv) the method allows for the quick selection of process parameters. The main disadvantage is that the flow stress, strain, and strain rate are assumed to be uniform for each elemental strip.

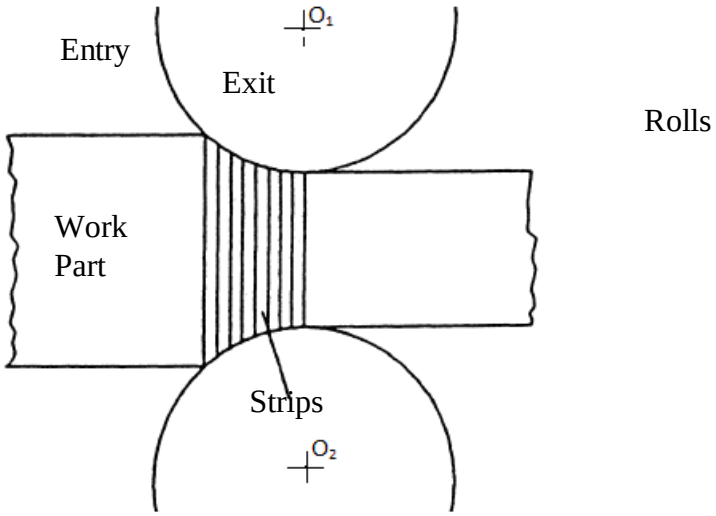

Figure 2.1. Slab or Strip Modeling of Rolling Process

2.3 Determination of Friction Coefficient

The mechanics of friction are complex, and the fundamentals of the phenomenon have been the subject of considerable study. Nevertheless, very little is known that would facilitate the formulation of the exact functional relationship between the friction force and the process variables. With the progress made in the understanding of metal forming processes and with the development of mathematical analysis tools, the role of friction force becomes more obvious. While there is a reasonable understanding of the mechanisms of friction at the roll work piece interface during cold rolling, the actual magnitude of the friction force is still largely a matter of conjecture.

Roberts [Roberts, 1997] made a comment regarding friction in rolling: "of all the variables associated with rolling, none is more important than friction force in the roll

bite angle". Friction in rolling, as in much other mechanical process, can be a best friend or a mortal enemy and its control within an optimum range for each process is essential. This research believes that to effectively control the rolling operation, an accurate knowledge of the friction coefficient within the contact region is required. Consequently, the ability to accurately measure the friction coefficient at the roll and part interface during the slab rolling operation becomes critical.

In slab rolling, the ratio of the interfacial frictional stress to the normal pressure is defined as the frictional coefficient. There are several ways to describe this friction coefficient. These include: (1) Coulomb Friction, where the frictional stress, (τ), is proportional to the pressure (P) between the work piece and the roll. Thus, $\tau = \mu P$, where the proportionality term "μ" is called the coulomb coefficient of friction. The coefficient of friction, (μ), is normally incorrectly assumed to be constant at all points between the roll and the work part interface [Avtzur, 1980]. (2) Amonton's Friction, where the frictional stress, (τ), is proportional to the shear yield strength (K) of the material. Thus, $\tau = mK$, where the proportionality factor "m" is called the shear factor, which is a constant multiplier between zero and unity [Liu, 2001]. While both of these approaches lead to reasonable predictions of the cold rolling process variables, they have been thought to be incorrect. A review of work done has revealed that the ratio of the frictional stress to the normal stress is indeed not constant during slab rolling, confirming that coefficient of friction varies from point to point between the roll and the work part interface.

2.3.1 Current Modeling Results

Several researchers have investigated the nature of the coefficient of friction in terms of some of the significant parameters, in the rolling process. These are usually in terms of the roll separation force, the radius of the deformed roll, the resistance to deformation, the entry thickness, and the exit thickness. Most of these results relied on matching the measured and calculated roll separation force and iterating on the coefficient of friction to allow for the match. One of the most popular models is given by Hill (1953) as in Equation 2.1.

$$\mu = \frac{\frac{P_r}{\bar{\sigma}\sqrt{R'\Delta h}} - 1.08 + 1.02\left(1 - \frac{h_{exit}}{h_{entry}}\right)}{1.79\left(1 - \frac{h_{exit}}{h_{entry}}\right)\sqrt{\frac{R'}{h_{entry}}}} \tag{2.1}$$

where, P_r is the roll separating force per unit width, $\bar{\sigma}$ is the average plane strain flow strength in the pass and R' is the radius of the flattened roll [Lenard, 2002]. Examination of Hill's formula shows that the friction coefficient (μ) is in terms of the entry and exit the thickness, roll separation force, average flow stress, and deformed roll radius. Since the pressure distribution varies within the contact region, the roll separation force is expected to vary, and so will the flow stress. Consequently, averaging the flow stress might not be a true reflection of the rolling operation. Moreover, the roll separation force and the deformed roll radius are input parameters that can only be determined through measurement. Furthermore, the value of the friction coefficient would be constant. The challenge in determining roll separation force and deformed roll radius prompted further research work.

Avitzur [Avitzur, 1964] sought to address the challenge in determining the roll separation force and the deformed roll radius in Hill's friction coefficient formula. He used the energy method to derive an expression for estimating the friction coefficient in terms of the rolling geometrical parameters and material properties. Avitzur's expression which is shown in Equation 2.2 is in terms the entry and exit thicknesses, the roll radius, the back and front tensions, and the yield strength of the work material.

$$\mu = \frac{\frac{1}{2}\sqrt{\frac{t_f}{R_0}}\left\{\ln\left(\frac{t_0}{t_f}\right)+\frac{1}{4}\sqrt{\frac{t_f}{R_0}}\sqrt{\frac{t_0}{t_f}-1}+\frac{\left(\sigma_{xb}-\sigma_{xf}\right)}{\left[2/\sqrt{3}\,\sigma_0\right]}\right\}}{\left\{\left(\ln\frac{t_0}{t_f}-1\right)\frac{\sigma_{xf}-\sigma_{xb}}{\frac{2}{\sqrt{3}}\sigma_0\sqrt{\frac{t_0}{t_f}-1}}-\left[\frac{1}{\frac{2}{\sqrt{3}}\sigma_0}\left(\sigma_{xb}-\frac{\sigma_{xf}-\sigma_{xb}}{\frac{t_0}{t_f}-1}\right)-1\right]\tan^{-1}\sqrt{\frac{t_0}{t_f}-1}\right\}} \quad (2.2)$$

Avitzur succeeded in dealing with the difficulty in calculating the roll separation force and the deformed roll radius in Hill's formula. He also introduced back and front tensions in his estimation, and assumed a constant flow stress within the contact region. Unfortunately, the estimation of friction coefficient within the contact region also resulted in a constant value.

Roberts developed an empirical relationship for the coefficient of friction in terms of the roll separating force (P_r), the radius of the flattened roll (R'), the reduction (r), the average of the tensile stresses at the entry and exit (σ_1), the average flow strength of the metal ($\bar{\sigma}$), and the entry thickness of the strip (h_{entry}) [Lenard, 2002]. The relationship is shown in Equation 2.3. Even though Roberts introduced a new parameter (tensile stress

at entry), the challenges in Hill's formula were not addressed. Roberts' parameters were similar to Hill's and also resulted in a constant friction coefficient within the contact region.

$$\mu = 2\sqrt{\frac{h_{entry}}{R'r}}\left[\frac{P_r(1-r)}{\bar{\sigma}-\sigma_1}\sqrt{\frac{1}{R'h_{entry}r}}-1+\frac{5r}{4}\right] \tag{2.3}$$

Ekelund also developed an empirical formula for estimating the friction coefficient as shown in Equation 2.4. The formula, which has similar rolling parameters as Hill and Roberts, is in terms of the roll separation force (P_r), the material properties, and the geometrical parameters of the rolling contact element [Lenard, 2002].

$$\mu = \frac{\left[\left(\frac{P_r}{\bar{\sigma}\sqrt{R'\Delta h}}-1\right)\left(h_{entry}+h_{exit}\right)+1.2\Delta h\right]}{1.6\sqrt{R'\Delta h}} \tag{2.4}$$

Ekelund's formula faced the same challenges as Hill and Robert. Again, Ekelund's formula uses entry and exit thicknesses and the friction coefficient within the contact region resulted in a constant value.

Tieu [Tieu et'al, 2005] investigated the relationship of the factors involved in the roll force calculation based on the Bland, Ford, and Hill's friction coefficient models. The deformation resistance and the friction coefficient were determined simultaneously by minimizing the error of the measured and calculated rolling forces using nonlinear least square optimization algorithm. The general equation proposed to describe the friction coefficient was $\mu = (a+bh+cr)\frac{d}{1+eN_r}$, where a, b, c, d, and e are coefficients, N_r , h, and r are the length of coil (length of rolled part), the exit thickness, and the

reduction respectively. The optimization method used Steel Material, N_r = 3000km, R = 270mm, $\Delta h = h_0 - h = 1.96$mm, $r = \frac{h_0 - h}{h}$ as the input parameters. The resulting friction coefficient model under these conditions is shown in Equation 2.5.

$$\mu = (0.01469 + 0.0298h + 0.00167r)\frac{1.09979}{1 + 0.000929N_r} \tag{2.5}$$

From the model, friction coefficient is in terms of the geometrical parameters. According to the authors, the material resistance which is given in terms of the length of coil accounts for the material property. Tieu's model is also in terms of the entry and the exit thickness. The friction coefficient within the contact region also resulted in a constant value.

Several other researchers in their contribution towards improving the estimation of the coefficient of friction use the following methods: (1) Experimental Method, in which the shearing and normal forces are monitored in the contact region and their ratios calculated; (2) Inverse Method, in which the coefficient of friction is computed using mathematical models of the rolling process. These methods are discussed below.

2.3.2 Experimental Method

The experimental method has been useful in estimating the coefficient of friction between the roll and part. One of the techniques [Lenard, 2002] involves the mounting of pressure measuring pins on the surface of the rolls. The roll pressures and the interfacial shear stresses are measured by pins and combination of transducers. The embedded pins and transducers in the segments of the roll body are shown in Figures 2.2 and 2.3.

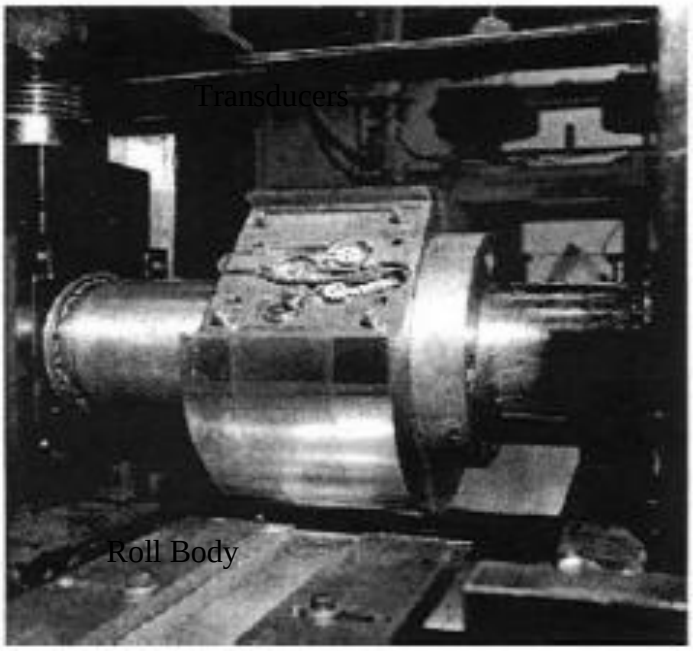

Figure 2.2. Picture Showing Embedded Transducers

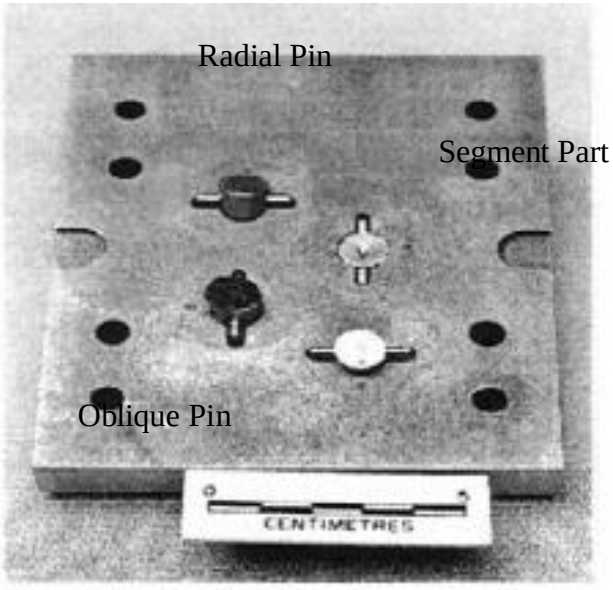

Figure 2.3. Picture Showing Measuring Pins

The transducers and the embedded pins placed in the segments which when assembled, complete the work roll surface. During rolling, the pins sense and pick a pressure signal which is relayed to the transducer. The transducer then converts the signal into a detectable output. The output is converted into force parameters. A force analysis of the signals from the pins, and the transducers yields the roll pressures and the shear stresses. The coefficient of friction is derived from these two quantities.

Even though the experimental method estimates friction coefficient as a function of roll angle, the experimental set-up is complex and expensive. There is also a high possibility of contamination (such as wear debris, aluminium oxides, particles or pieces of scaling) intruding into the clearance between the pins and their housing, thus affecting the reliability of the results.

Several attempts have been made to measure the normal and frictional stresses between rolls and workpart during rolling. Siebel and Lueg were among the first experimenters who attempted to measure the normal pressure in the deformation zone using pressure measuring pins. A pin supported by a piezoelectric ceramic was mounted in a radial hole and extended at 0.01mm outside the roll surface. In the experiments, a piezo-electric crystal with a suitable detecting equipment was used, but a very substantial correction factor was needed for the experiments due to the large ratio of pin width to contact length. The normal pressure was measured by calibrating the electrical output from the piezoelectric ceramic. According to the authors, a neutral point was clearly identified and a drop in pressure towards the exit of the strip was found [Siebel, 1933].

The large ratio of pin width to contact length prompted further research work. Consequently, Rooyern and Backofen developed a technique aimed at reducing the contact ratio by measuring tangential and normal stress within the contact region. The procedure made use of two pressure measuring pins, the one for normal pressure measurement being installed in the radial direction and the other pin termed the oblique pin inclined in the rolling direction at an angle to the radial pin. Figure 2.4 is a schematic of the measuring device. This concept enabled the separation of the normal pressure from the frictional stress. According to the authors, both the radial and the oblique pin techniques were found to be useful tools for exploring frictional conditions within the contact region [Rooyen et'al, 1957]. Although Rooyen's technique required a high accuracy of measurement in the placement of the oblique pin, it had a great potential and with refinements could yield good results.

Figure 2.4. Rooyen's Measurement Technique

An improved pin technique was developed by Al-Salehi [Al-Salehi et'al, 1973], with the aim of obtaining reliable measurements of the frictional stress within the contact region. The approach used an instrumented roll, designed with the provision to accommodate two pressure transducers. The details are shown in Figure 2.5. Two holes were drilled through the roll at right angles to the roll axis, one in the radial direction and the other inclined to the first hole in an oblique direction.

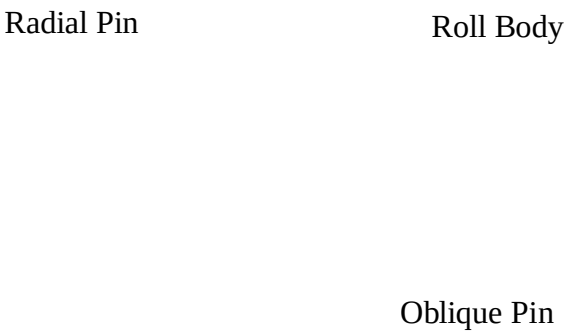

Figure 2.5. Al-Salehi's Measurement Technique

Their centers were spaced apart on the same line parallel to the roll axis. According to the authors, roll loads calculated from the measured normal pressure were in close agreement with the roll separating force measurement. Moreover, the roll torque measured agreed with the calculated value. Even though the authors' results showed

variation of the friction coefficient within the contact region, the measurement of frictional stress using the oblique pin required some allowance for tangential deflection. This research work sought to focus on frictional stress measuring technique with the provision for the tangential deflection.

The pin technique was further improved by Truncer and Dean (1987), who used a conical pin that fits in a conical housing in the roll. This principle enhanced the point measurement within the contact region, and also prevented the material from penetrating the holes in the roll even at high pressures. Lenard (1993), used the improved pin technique and found out that the peak in the normal pressure may occur at a point different from the neutral point. Later, Lagergren [Lagergren et'al, 1997] identified a double normal pressure peak using this technique. These revelations by Lenard and Lagergren suggested that the pin technique was very effective in measuring normal pressure.

Jeswiet introduced a measuring technique in which a work roll used strain gages mounted on a conical cantilever as a sensing element. His contention was that one pressure transducer in a form of a conical cantilever located radially into the work roll could measure the normal pressure and the frictional stress in both the rolling and the orthogonal directions. Figure 2.6 shows this technique. Jeswiet's technique eliminated the oblique pin, and also introduced another component of the frictional stress in the orthogonal direction which earlier researchers did not take into account. According to the author, successful experiments have been conducted with the instrumented roll on a laboratory rolling mill equipment. Results showed that the friction coefficient could be

measured successfully [Jeswiet, 1993]. Even though the author's results showed the variation of friction coefficient within the contact region, the measurements of normal pressure using the conical cantilever technique lacked precision.

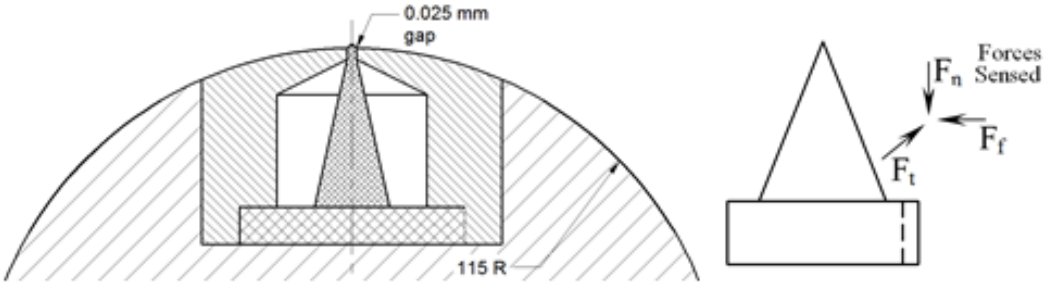

Figure 2.6. Jeswiet's Measurement Technique

Tieu and Liu introduced four pin transducers in the pin measuring technique. In order to embed the pin transducers into the roll body, the roll was segmented into two parts along the axial direction as shown in Figure 2.7. The segmented rolls were held tightly together by bolts and dowel pins. On the separating surface of the roll body, dowel pins guided the segmented parts into the proper position. Two of the transducer pins were radial pins and located along the radial direction while the other two pins were oblique pins and inclined at an angle to the radial pin. The pin diameter was relatively small compared to the other pin measuring techniques. The variation of friction coefficient within the contact region was detected. Figure 2.8 shows the experimental results obtained from the experimental data [Tieu, 2004].

Figure 2.7. Tieu's Measurement Technique

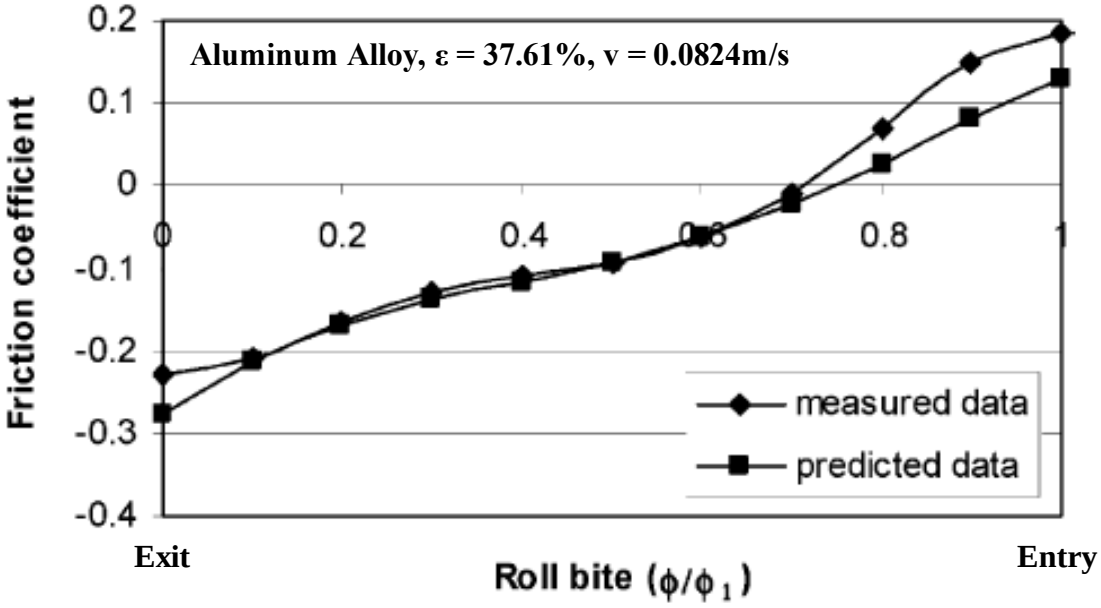

Figure 2.8. Tieu's Experimental Results

According to Tieu's experiment, the coefficient of friction can be empirically expressed by Equation 2.6.

$$\mu = -0.1912 - 0.5218X + 4.8515X^2 - 14.2263X^3 + 17.5845X^4 - 7.3474X^5 \quad (2.6)$$

where μ is the friction coefficient, X is dimensionless variable defined as $X = \phi / \phi_1$, and Φ_1 is roll bite. The negative portion shows a change in friction direction. The experimental results confirmed that the friction coefficient varied with roll angle. However, the nature of the friction coefficient model did not follow the physics of rolling. There was no identifiable "no-slip" point. Also, the experimental set up and the data acquisition system were sophisticated and costly. This research work sought to design a simpler and less expensive friction coefficient measuring technique.

2.3.3 Inverse Method

Inverse calculations have been used to estimate the coefficient of friction. The technique requires that some of the parameters of the process are measured experimentally and others determined by mathematical models. A model is assumed and the coefficient of friction parameter in the model is adjusted until the measurement and predictions match to within an acceptable tolerance. It is understood that increasing the number of measured and calculated parameters to be matched increases the prediction accuracy.

Gelin and Ghouati [Gelin, 1995] estimated the friction coefficient using the inverse method. The authors combined a finite element simulation of a rolling process with the measurements of rolling parameters. The measured parameters were compared

with the predictions from the finite element method. The measured and predicted results matched within the acceptable tolerance. The method was effective but predicted a constant coefficient of friction.

2.4 Analysis Using FEM

Several researchers have contributed to the scientific knowledge in the field of metal forming in relation to cold rolling processes using FEM. Liu by means of a 3-D elastic-plastic FEM, simulated the cold strip rolling process in a 4-high rolling mill. The paper entitled "FEM Analysis of Rolling Pressure along Strip Width in Cold Rolling Process," took into account the elastic deformation of rolls, the plastic deformation of the strip, and the pressure between the work roll and the backup roll to obtain the distribution of rolling pressure along the strip width. Based on simulation results, the peak value of the rolling pressure and its location were obtained under different rolling conditions. According to the authors, the effects of the roll bending force and the strip width on the distribution of the rolling pressure along the width direction were determined [Liu, 2007].

Gao [Gao et'al, 2002] did research work in asymmetrical cold rolling produced by the difference in the coefficient of friction between rolls and sheets rather than the difference in roll radius or rotational speeds. The authors in their paper entitled "Analysis of Asymmetrical Cold Rolling with varying Coefficients of Friction," investigated the influence of the friction coefficient ratio on the cross shear deformation, rolling pressure and torque, using the finite element modeling method. The results showed that the shear deformation zone length increased with the increase in the friction coefficient. As the

reduction per pass was increased, the shear deformation zone length increased and the rolling force also increased. An increase in the front tension resulted in a decrease in the shear deformation zone length. An increase in the back tension, however, led to an increase in the shear deformation zone length. According to the authors, the reduction of rolling torque for the work roll with higher surface roughness was greater than that for the work roll with lower surface roughness.

Jeswiet [Jeswiet, 1995] published a paper entitled "Aspect Ratio, Friction Forces and Normal Forces in Strip Rolling". The procedure used a sensor to measure normal and friction forces at the contact interface in the cold rolling of aluminum. The results revealed that the friction force was not constant within the roll gap but varied with time. The author successfully used the sensor to conduct a series of experiment at several different aspect ratios, with the intention of observing the effect of aspect ratio on the friction force. According to the author, the results of the experiments revealed that the friction force was not constant throughout the roll gap.

Le and Sutcliffe [Le, 2001] developed a technique for analyzing cold rolling of thin strip and foils using the finite element modeling method. Their model followed the approach of [Fleck et'al, 1999], but they relaxed their assumption of a central flat neutral zone. Instead of following the inverse method to obtain the pressure distribution in the neutral zone, an explicit function for the contact pressure variation was obtained from the sticking condition in this region. This significantly simplified the solution method, leading to a more robust algorithm. Moreover, the method dealt with situations with significant roll deformations. This facilitated the incorporation of other effects such as

the friction models. The authors claimed that their results were in line with Fleck's theory and used the results to investigate the effect of entry and exit tensions on the non-dimensional load and forward slip. For example, they found out that the effect of equal entry and exit tensions was equivalent to reducing the yield stress of the strip. This finding was very useful for modelling cold rolling using the strip or slab method.

Yuen [Yuen et'al, 1996] verified the numerous mathematical models developed at various research laboratories to study the flat rolling processes. Their paper discussed models developed for the examination of the plastic deformation of the work piece in the roll bite zone. Depending on the rolling regime, models of different complexities were required to accurately predict the strip and roll deformations. The paper covered models ranging from hot rolling to skin pass rolling, and from very high to extremely low reductions. According to the authors, comparisons of the results with experimental values confirmed the validity of the models.

Kumar [Kumar et'al, 2005] concluded that both the finite element method and the numerical integration techniques were capable of predicting roll force and roll torque values with sufficient accuracy during cold rolling of sheets, metals, and strips. In their paper entitled "Analysis of Strip Rolling using Finite Element Method and Numerical Integration Techniques," strip rolling of isotropic material was analyzed under plane strain conditions using the finite element analysis technique for the elasto-plastic case. The objective of the study was to predict the roll force and roll torque necessary for the deformation of the work piece. The incremental approach was adopted for obtaining the required elasto-plastic stress-strain matrix. Similar analysis has been carried out by means

of the numerical integration method considering the pressures before and after neutral point. Simpson's one third rule was applied and the roll force and the roll torque were computed. The authors developed two empirical equations for the estimation of roll force and torque.

Zone-Ching Lin and Ven-Huei Lin [Lin, 1995] developed a three-dimensional thermo-elastic plastic finite-element model coupled with a three dimensional heat-transfer finite-difference model under the assumption of rigid work and rolls. Their paper entitled "Analysis of the Variation of the Cold-Rolling Characteristics of Rolling Force, Strip Shape, Stress and Temperature, for a Three-Dimensional Strip," simulated the cold rolling process using a numerical method. The goal of the authors was to explore the phenomena that could not be understood by means of a two-dimensional simulation, such as the shape changes, the force distribution, and the distribution of the stress and temperature on both surfaces of a three-dimensional strip. According to the authors, there was a bulge on the strip sides during rolling, the largest amount of bulging being about 0.2 mm, occurring at the node after the exit from the contact area. The presence of waves on the external surfaces had an adverse impact on the quality of the strip.

2.5 Analysis Using the Slab Method

The Slab or strip method for modeling of the cold strip rolling process predicts the pressure distribution by analyzing the forces acting on each strip. The theory of homogeneous deformation suggested by Von Karman was based on simplified equilibrium of forces acting on a slab element in the deformation zone. Orowan

discarded the assumption of homogeneous deformation and developed a theory of inhomogeneous deformation [Orowan, 1943]. The differential equation for slab element was derived under various assumptions and approximations by other researchers. Several research work have been done in estimating roll force, roll torque, and pressure distribution during cold rolling processes. This research work was directed toward the effects of friction along the arc of contact.

Liu [Liu et'al, 2001] studied friction in the roll bite region under laboratory conditions using a roll with embedded pins. The studies targeted rolling parameters such as the friction force and pressure under dry and lubricated conditions using aluminum alloy as the material to be rolled. The authors in the paper entitled "Friction Measurement in Cold Rolling," concluded that the sensor roll (work roll with embedded pins) could give a reliable friction measurement. The results confirmed that the friction coefficient in the roll bite was not uniform. They also validated their experimental results with theoretical results. This research work seeks to develop a technique which evaluates the friction coefficient as a function of the roll angle.

Tieu [Tieu et'al, 2005] contended that the rolling force model required an accurate knowledge of the deformation resistance of the material and a proper friction coefficient calculation. In their paper entitled "Material Resistance and Friction in Cold Rolling," the main interest was to investigate the relationship of the factors involved in the roll force calculation based on the Bland-Ford-Hill model. The deformation resistance and friction coefficient were determined simultaneously without relying on empirical data of material resistance. Eight coefficients in the material resistance and friction coefficient

models were derived by minimizing the error of the measured and they calculated the rolling forces based on nonlinear least squares optimization method. The effect of the work roll wear and the rolling speed on the friction coefficient in the roll bite were analyzed. According to the authors, the friction force decreased with roll wear, and the lower the rolling speed, the higher is the friction. Even though Tieu advocated for proper friction coefficient calculation, a careful examination of their model coefficients and variables revealed that the value of the friction coefficient generated was constant. A realistic model for a friction coefficient along the roll work piece interface in the analysis of strip rolling was one that made friction coefficient a function of roll angle. This research work seeks to develop a technique in that direction.

Abdollahi and Dehghani [Abdollahi, 2007] strongly believed that the rolling process was one of the most important ways of metal forming. They contended that, since the results of this process were almost finished product, controlling the parameters affecting rolling process was very important in order to have cold rolling products with high quality. Among the parameters considered, the coefficient of friction within the roll gap was the most significant one. They further explained that, since other rolling parameters such as rolling force, pressure in the roll gap, forward slip, surface quality of sheet, and the life of work rolls were directly influenced by friction, a true value of the friction coefficient was paramount. In their paper entitled "Study of Friction Distribution during the Cold Rolling of Material by Matroll Software," a new software dubbed Matroll, was introduced to determine the coefficient of friction and to plot the friction hill for an industrial mill. Besides the rolling equations used in the development of the

program, the software offered about 30 rolling parameters as outputs. Having the rolling characteristics as inputs, the software was able to calculate the coefficient of friction. According to the authors, many rolling passes were performed on real industrial mill and the coefficient of friction was obtained for all passes. The results were in good agreement with the findings of other researchers. Once again, the equation used by the authors in the program for the determination of a true value of friction coefficient resulted in a constant value.

Abdollahi and Dehghani [Abdollahi, 2008] again published a paper entitled "Irregularity in Friction Hills during the Cold Rolling of Materials". They maintained that among the cold rolling parameters, the pressure distribution or friction hill within the roll gap was of the greatest concern. The authors revealed that almost all of the previous research in investigating the effects of the friction coefficient along contact arc or work roll interface was based on laboratory simulations rather than an industrial mill conditions. In this study, following the determination of the coefficient of friction, the friction hills for the real industrial mills were obtained. After carrying out various industrial cold-roll passes on aluminum alloy and low carbon steel, the friction hills were plotted for industrial cases. According to the authors, there were irregularities in the real industrial friction hills and were different from those reported for laboratory cases. The authors believed that the irregularities accounted for low values of friction coefficient during the industrial rolling process. A true friction value developed as a function of roll angle might address this discrepancy.

Lenard [Lenard, 2004] investigated the effects of the roughness of the work roll on the force, torque, and the forward slip during cold rolling process. In a paper entitled "The Effect of Roll Roughness on the Rolling Parameters during Cold Rolling of an Aluminum Alloy," the author used light mineral seal oil with 5% alcohol as a lubricant to cold roll 6061-T6 aluminum alloy strips at various speeds and various reductions. The roll roughness, obtained by sand blasting was varied from a low of 0.3 to a high of 2.4μm. The roll separating force, roll torque and the forward slip were measured. The coefficient of friction was calculated by Hill's formula and the friction factor was evaluated by using the upper bound approach. The process conditions were studied and the frictional force mechanisms were identified. According to the author, high roughness appeared to increase the possibility of insufficient lubrication at the interfaces. While both adhesive and ploughing forces were present in all instances, the ploughing forces became dominant at higher rolling speeds. The contribution of ploughing to the frictional resistance increased as the roll roughness increased to a certain value and beyond that value, its behavior depended on the rolling speed.

Judging from the above research reviews, it can be said that: (1) the finite element solutions are capable of providing better simulations of metal forming processes, (2) the slab or strip method can provide a better estimation of pressure distribution over the contact, (3) further research is needed to study the variation of the friction coefficient along the arc of contact of the roll- strip interface.

CHAPTER 3

METHODOLOGY AND DATA ACQUISITION

The existing friction coefficient models have the following characteristics: (1) they use only the entry and the exit thicknesses of the work part, (2) they have input parameters which are difficult to obtain, (3) they approximate flow stress to be constant within contact region, and (4) they result in a constant coefficient of friction value. There is, therefore, the need to continue to search for a friction coefficient model within the contact region that obeys the laws of friction and is easier to estimate. This work investigates the friction coefficient as a function of roll angle and seeks to address the above needs by modifying Avitzur and Tieu's models. This chapter discusses modified modeling techniques and the experimental data needed to verify the models developed.

3.1 Proposed Modified Modeling Technique

The current modeling techniques assume several constant parameters in the contact region and estimate the friction coefficient using only the entry and exit conditions. Figure 3.1 illustrates the characteristics of the current modeling input parameters where h_0 is the entry slab thickness, h_f is the exit slab thickness, R_0 is the roll radius, and θ_{max} is the maximum included angle.

This work proposes to section the contact region into piecewise strips of varying thicknesses and then evaluates the friction coefficient at each strip. Since the centers of the two rollers are fixed, the exit thickness is used as the reference.

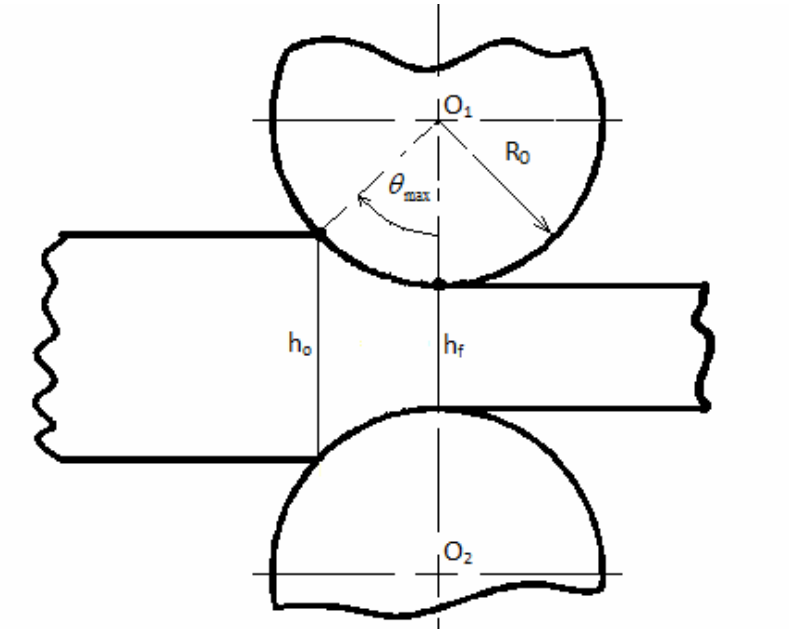

Figure 3.1. Current Modeling Technique

Figures 3.2 and 3.3 illustrate the proposed modified modeling technique. The roll angle is also measured from the reference line and its incremental direction is also shown in Figure 3.3. The symbols h_i and h_{i+1} represent the exit and entry thicknesses respectively for the i^{th} elemental strip. Given the roll radius (R_0), the entry thickness (h_n) or exit thickness (h_0), and the maximum reduction (r), the roll included angle (roll bite angle) can be calculated from the geometry of the arc contact. For each incremental angle, the corresponding incremental thickness can be evaluated using Equation 3.1. The present friction coefficient models are then developed based on the elemental strips.

$$h_{i+1} = h_i + 2R(1-\cos\theta_i) \tag{3.1}$$

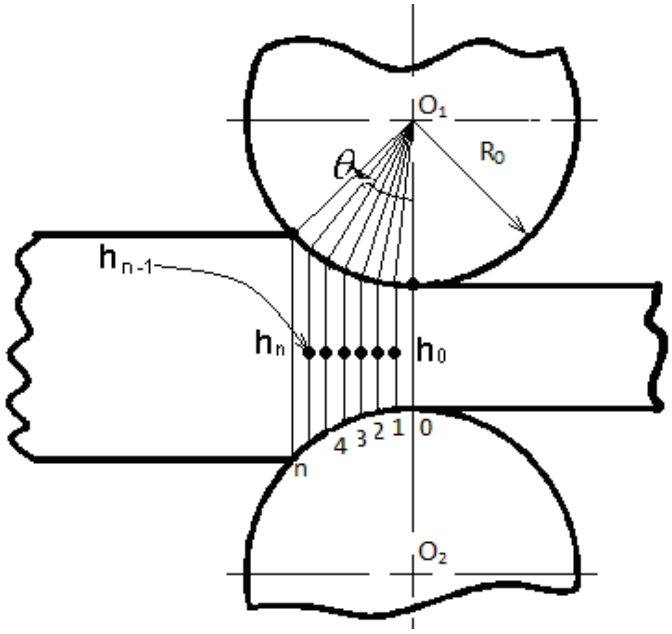

Figure 3.2. Modified Modeling Technique Showing "n" Steps

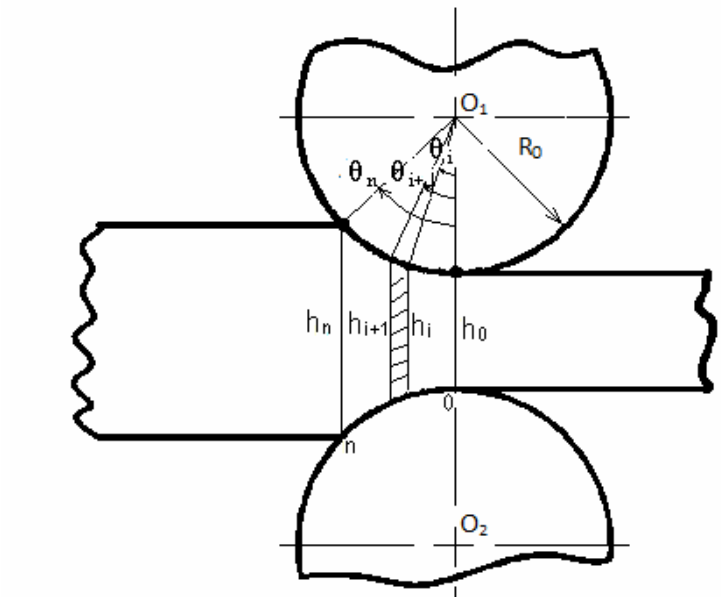

Figure 3.3. Modified Modeling Technique Showing an i^{th} Element

3.1.1 Modification of Tieu's Model

Tieu's friction coefficient model was modified to assume the difference equation form as shown in Equation 3.2.

$$\mu_i = \left(0.01469 + 0.0298\, h_i + 0.00167\, r_{i+1}\right)\frac{1.09979}{1 + 0.000929\, N_{i+1}} \tag{3.2}$$

The proposed modeling technique was demonstrated using an illustrative example with the following parameters: Roll Radius (R_0 = 270mm), draft ($\Delta h = h_n - h_0 = 1.96$), and aluminum alloy as part material. From the input parameters, the maximum roll angle (bite angle) was calculated to be 0.08 radians. Then, starting from the reference angle (0^o) and incremental angle of 0.005 radians was used to evaluate the corresponding incremental thicknesses and friction coefficients using Equations 3.1 and 3.2 respectively. This was done using a Matlab Program developed for this research (Appendix B).

The output from the Matlab Program is presented in Table 3.1 and Figure 3.4. It can be seen from Figure 3.4 that, the friction coefficient decreased rapidly from a maximum value of about 0.12 to a given point beyond which it decreased slowly as the work exited the roll. This occurrence was consistent with the principle of physics in that friction force between surfaces in contact decreased continuously as the part transitional from quasi static to dynamic mode. Also, Tieu's experimental results showed a favorable comparison with the Modified Tieu Model.

Table 3.1. Output of Modified Tieu Friction Coefficient Model

Roll Angle (θ_i) - radians	Instantaneous Parameter	
	Part Thickness (h_i) - mm	Friction Coefficient (μ_i)
0.00	25.00	0.0817
0.01	25.03	0.0820
0.02	25.11	0.0829
0.03	25.24	0.0848
0.04	25.43	0.0881
0.05	25.67	0.0930
0.06	25.97	0.0999
0.07	26.32	0.1092
0.08	26.73	0.1213
0.09	27.19	0.1331

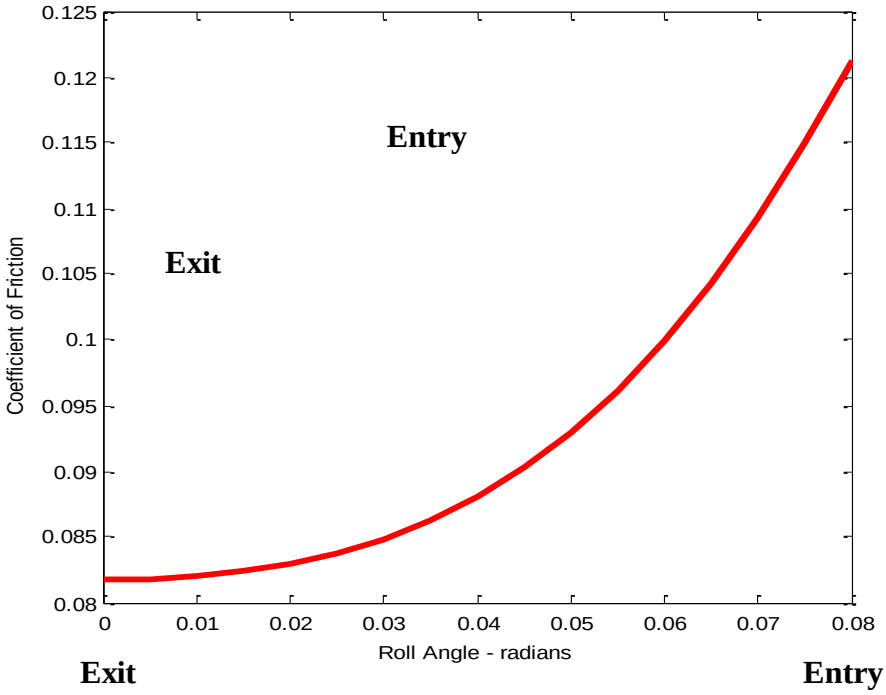

Figure 3.4. Friction Coefficient versus Roll Angle – Modified Tieu

Using another Matlab Program developed for this research, (Appendix B), the exact discontinuity point was identified to be at a location of $\theta = 0.0184$ radians from the exit of the roll. The logic behind the Matlab Program is as follows: (1) provide a relationship between the friction coefficient and the roll angle (Figure 3.4, $\mu = f(\theta)$), (2) locate the region of discontinuity, (3) from entry of $\mu = f(\theta)$ to the region of discontinuity, fit a curve named $\mu_{before} = f(\theta)$, (4) from exit of $\mu = f(\theta)$ to the region of discontinuity, fit a curve named $\mu_{after} = f(\theta)$, (5) for θ values within the region of discontinuity, find μ_{after} and μ_{before} such that μ_{after} is equal to μ_{before} within an arbitrary tolerance of 0.005. The point of discontinuity is assumed to be the no slip point. The value of θ which satisfies the condition is the location of the no-slip point and labelled θ_{NS}. The program flow chart is shown in Figure 3.5. The quantitative relationship between the friction coefficient and the roll angle was found for the curves before and after the no slip-point and are presented in Equations 3.3 and 3.4 respectively.

$$\mu_{Before} = 10.11\theta^2 - 0.3877\theta + 0.0871 \tag{3.3}$$

$$\mu_{After} = 0.083 \tag{3.4}$$

Tieu's model and the Modified Tieu model were compared and the results shown in Figure 3.6. The friction coefficient between the roll and work interface for original Tieu's model was found to be constant at approximately 0.086 for all the points of contacts until the work exited the roll, while the modified Tieu model revealed a variable friction coefficient ranging from a value of about 0.12 until the "no-slip" point of about 0.0182 radians was reached, and then followed by a slow decrease in its value until the work exited the roll at a friction coefficient value of about 0.082.

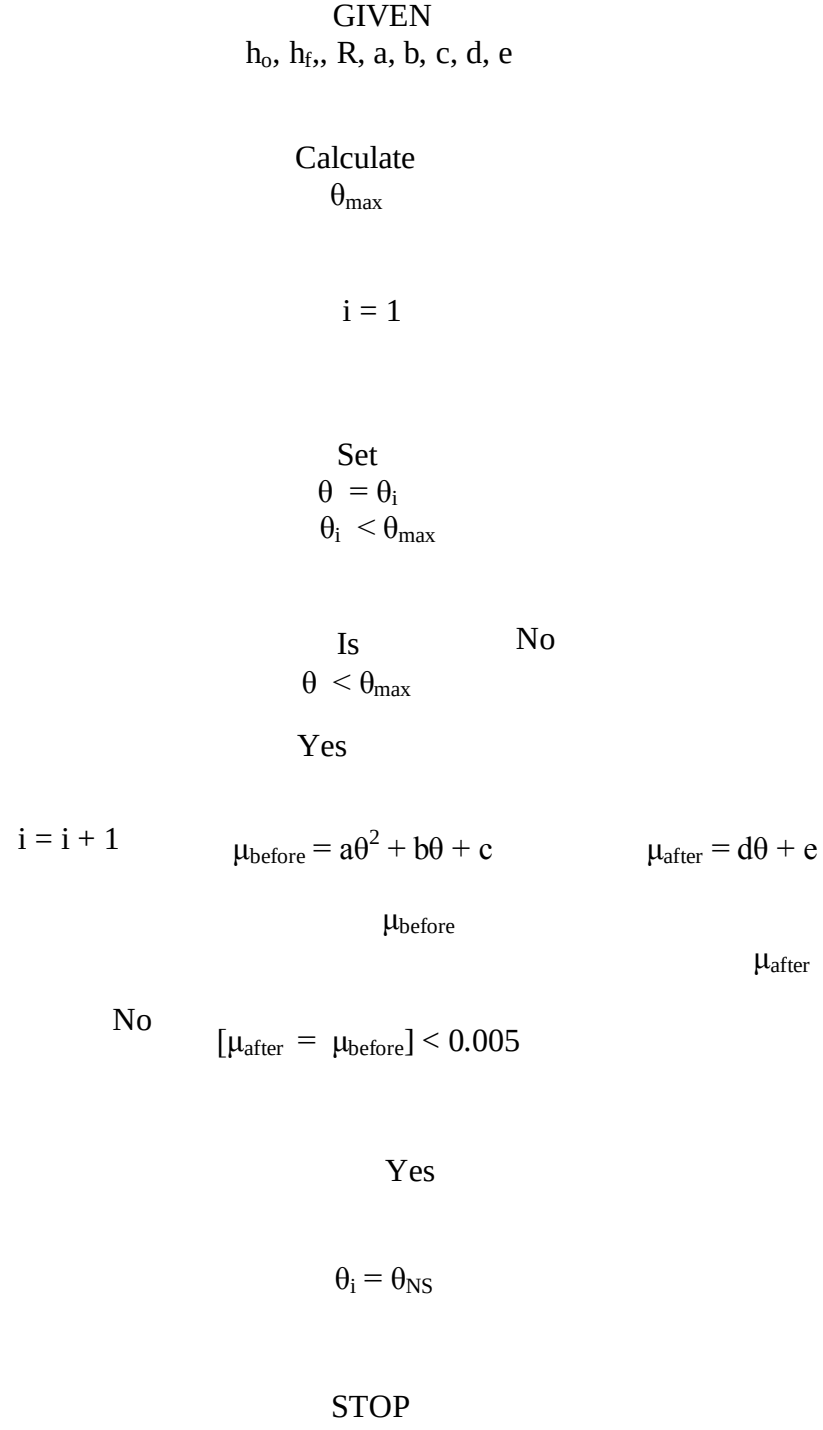

Figure 3.5. Flow Chart for Determination of No-Slip Point

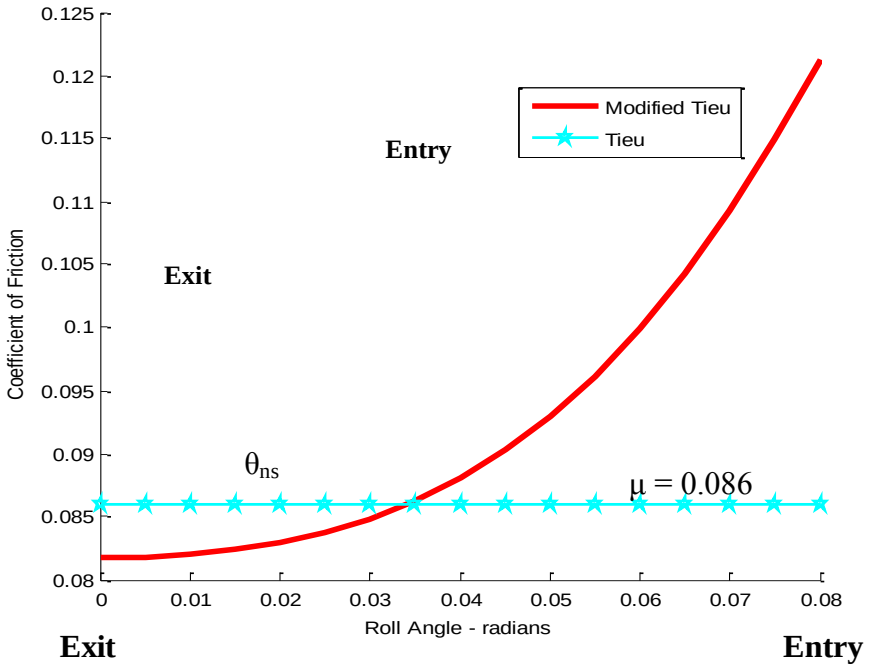

Figure 3.6. Comparison of Tieu and Modified Tieu Models

Tieu's model did not take into account the physics of contact rolling which suggested a change in the direction of the friction force at the point of no slip within the contact region. The manifestation of the physics in contact rolling must show some discontinuity in the graph of the friction coefficient against roll angle. The Modified Tieu model showed the expected characteristics of the behavior of friction within the contact zone.

3.1.2 Modification of Avitzur's Model

An analysis was performed for the case of Avitzur's model using the proposed piecewise strip technique. The resulting equation for the coefficient of friction is shown in Equation 3.5.

$$\mu_i = \frac{\frac{1}{2}\sqrt{\frac{h_i}{R_0}}\left\{\ln\left(\frac{h_{i-1}}{h_i}\right)+\frac{1}{4}\sqrt{\frac{h_i}{R_0}}\sqrt{\frac{h_{i-1}}{h_i}-1}+\frac{\left(\sigma_{xb}-\sigma_{xf}\right)}{\left[2/\sqrt{3}\,\sigma_0\right]}\right\}}{\left\{\left(\ln\frac{h_{i-1}}{h_i}-1\right)\frac{\sigma_{xf}-\sigma_{xb}}{\frac{2}{\sqrt{3}}\sigma_0\sqrt{\frac{h_{i-1}}{h_i}-1}}-\left[\frac{1}{\frac{2}{\sqrt{3}}\sigma_0}\left(\sigma_{xb}-\frac{\sigma_{xf}-\sigma_{xb}}{\frac{h_{i-1}}{h_i}-1}\right)-1\right]\tan^{-1}\sqrt{\frac{h_{i-1}}{h_i}-1}\right\}} \quad (3.5)$$

The modified modeling technique was demonstrated using the same input parameters as used in the previous analysis and a Matlab Program (Appendix B) developed for this research work. The procedure was the same as in section 3.1.1. The result is as shown in Table 3.2 and Figure 3.7.

Table 3.2. Output of Modified Avitzur Friction Coefficient Model

Roll Angle (θ_i) - radians	Instantaneous Parameter	
	Part Thickness (h_i) - mm	Friction Coefficient (μ_i)
0.00	25.00	0.0503
0.01	25.03	0.0923
0.02	25.11	0.1133
0.03	25.24	0.1256
0.04	25.43	0.1343
0.05	25.67	0.1418
0.06	25.97	0.1496
0.07	26.32	0.1585
0.08	26.73	0.1689
0.09	27.19	0.1692

From Figure 3.7, the friction coefficient decreased steadily from a maximum value of about 0.17 until the point of "no-slip" was attained. At this point, the friction coefficient decreased rapidly until the work part exited the roll. Using a Matlab Program

(Appendix B), the exact position of the no slip point was identified to be 0.022 radians from the exit of the roll.

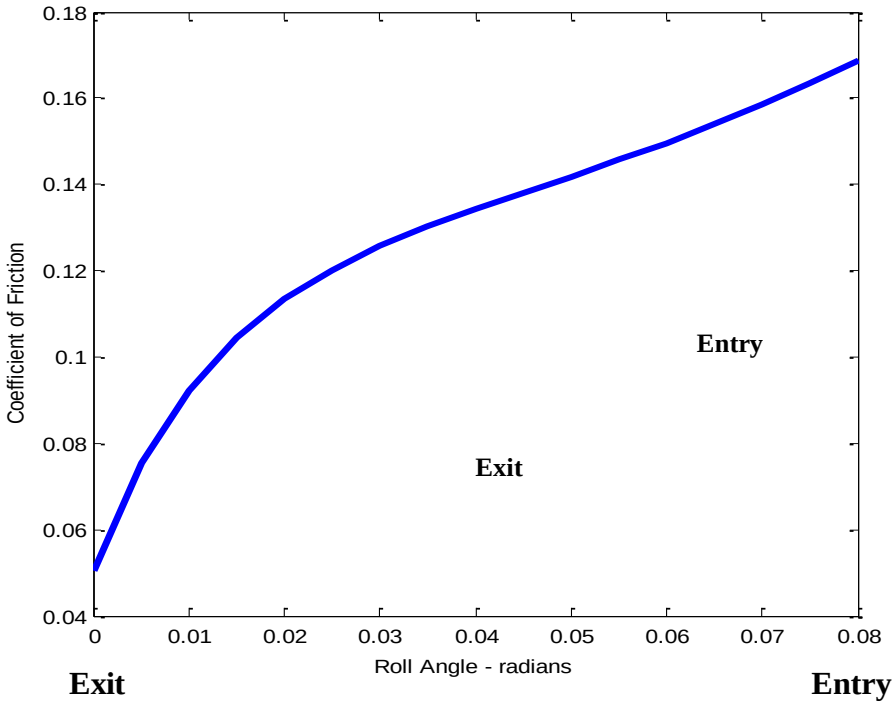

Figure 3.7. Plot of Friction Coefficient - Modified Avitzur Model

The mathematical relationship between the friction coefficient and the roll angle was found before and after the "no-slip" point and the results are presented in Equations 3.6 and 3.7.

$$\mu_{Before} = 0.8395\theta + 0.1002 \tag{3.6}$$

$$\mu_{After} = -106\theta^2 + 5.222\theta + 0.0508 \tag{3.7}$$

Avitzur's model and the Modified Avitzur model were compared and the result is shown in Figure 3.8. The friction coefficient between the interface of the roll and work part for Avitzur's model stayed constant at about 0.08 for all the points of contacts until the work exited the roll, while the Modified Avitzur model revealed a gradual decrease in friction coefficient value from about 0.17 until the no-slip point of about 0.022 radians from the exit, and then decreased rapidly until work exited the roll at a friction coefficient value of about 0.051. Once again Avitzur's model did not agree with the physics of contact rolling friction.

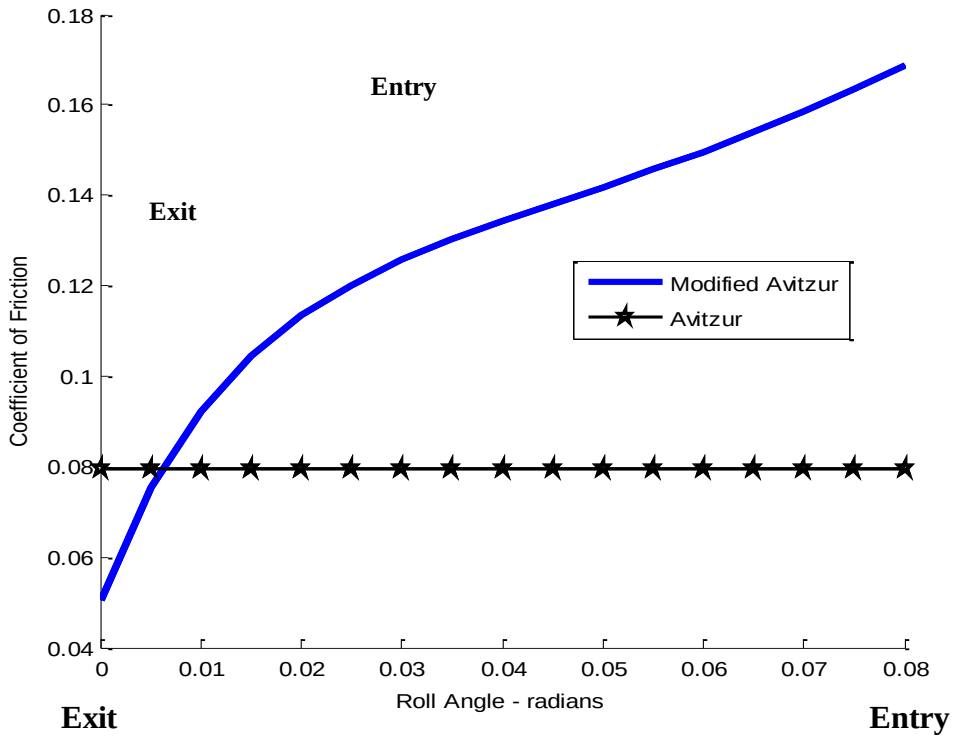

Figure 3.8. Comparison of Avitzur and Modified Avitzur Models

The proposed modified modeling technique involves the following steps:

i. calculate the roll bite angle (θ_{max}).

ii. decide the roll angle step size ($\Delta\theta$).

iii. evaluate the total number of angle points using the angle step size

iv. with the known exit thickness (h_0), calculate the next thickness (h_1) with its corresponding angle (θ_1) from Equation 3.6.

v. determine friction coefficient (μ_1) using modified friction coefficient models (Equation 3.7, Equation 3.10).

vi. repeat steps iii to v until $\theta = \theta_{max}$.

vii. plot friction coefficient (μ) versus roll angle (θ).

viii. from the plot, identify the "no slip" point.

viiii. determine friction coefficient as a function of roll angle before and after the "no slip" point.

The Modified Tieu and the Modified Avitzur models were compared and the result is as shown in Figure 3.9. As the work part made contact with the roll, Modified Avitzur model had a higher friction coefficient value than the Modified Tieu model for the same parameters. The situation was the same at the no-slip points but reversed as the work exited the roll. Both friction coefficient models showed discontinuities which was consistent with the physics of contact rolling friction. The discontinuity in the Modified Avitzur's Model was more pronounced than that of the Modified Tieu's Model.

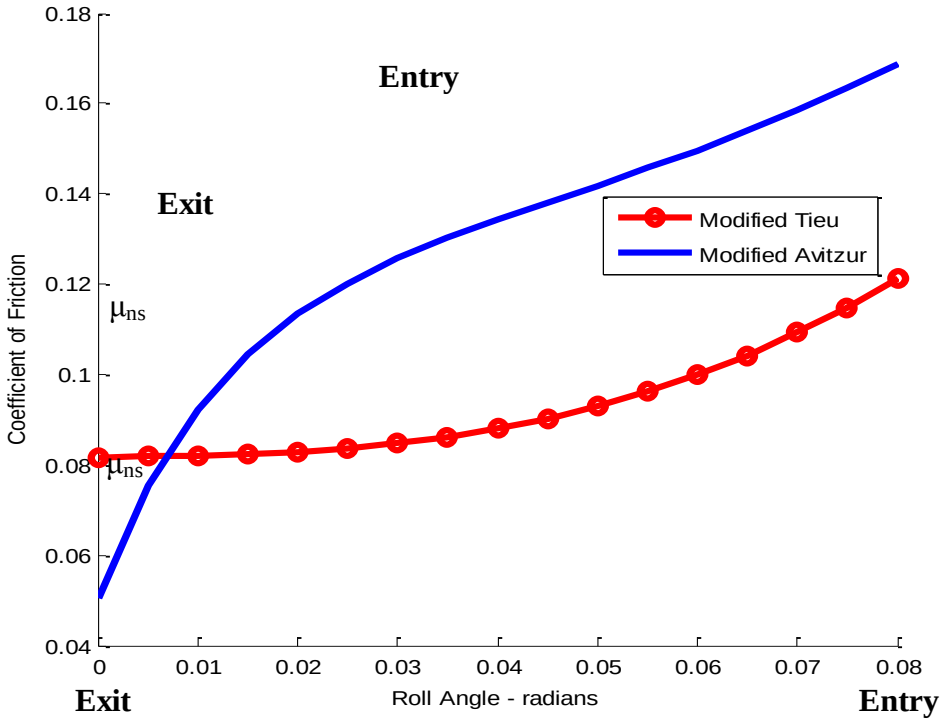

Figure 3.9. Comparison of Modified Avitzur and Modified Tieu Models

The obvious next step was to compare the two friction coefficient models with experimental data to verify which model best described the rolling process. The next section discusses the friction coefficient measuring technique, the experimental set up, and the data collection.

3.2 Friction Coefficient Measurement Techniques

This research considered the friction coefficient within the contact region as a function of the roll angle. This section seeks to collect experimental data to verify these modified models. To measure the instantaneous friction coefficient, it is necessary to know the normal force and the friction force at each point within the contact region. The

ratio of the frictional stress to the normal pressure is the friction coefficient. This research proposes and demonstrates a measuring technique for the normal force and the frictional force at sampled points in the contact region.

3.2.1 Proposed Measurement Technique

From the current friction coefficient measuring techniques, it was clear that the pin measuring technique received much attention. Nevertheless, the possibility of lateral deflections of the oblique pin tend to create contact between the pin and the inside surface of the hole. Consequently, the output of the transducer may include unpredictable errors into the measurement of the frictional stress. For the frictional stress measurement, the oblique pin needed some allowance for lateral deflections. This research work sought to modify the pin measuring technique through design changes of the instrumented roll. The improved instrumented roll referred to as the Strain Gaged (SGRoll) would be less expensive, would use simpler sensors, and would make provision for lateral deflection. The next section discusses the design of the SGRoll.

3.2.1.1 Design Features of SGRoll

Dimensions of the SGRoll were chosen to fit a two high roll laboratory rolling mill equipment. Details of the rolling mill equipment are presented in Section 3.2.1.3. As shown in Figure 3.10, the SGRoll is segmented into two parts along the axial direction in order to embed sensing elements into the roll body. The design details of the SGRoll are shown in Appendix C.

There were two sensing elements, namely, the radial sensing element and the tangential sensing element. The radial sensing element comprised of a conical pin, a

spherical ball, and a radial rectangular bar. The tangential rectangular bar made up the tangential sensing element. Strain gauges were bonded to the radial rectangular bar and the tangential rectangular bar for the measurement of rolling forces. Two holes were drilled on either side of the sensor roll to accommodate the transmitting wires from the strain gages.

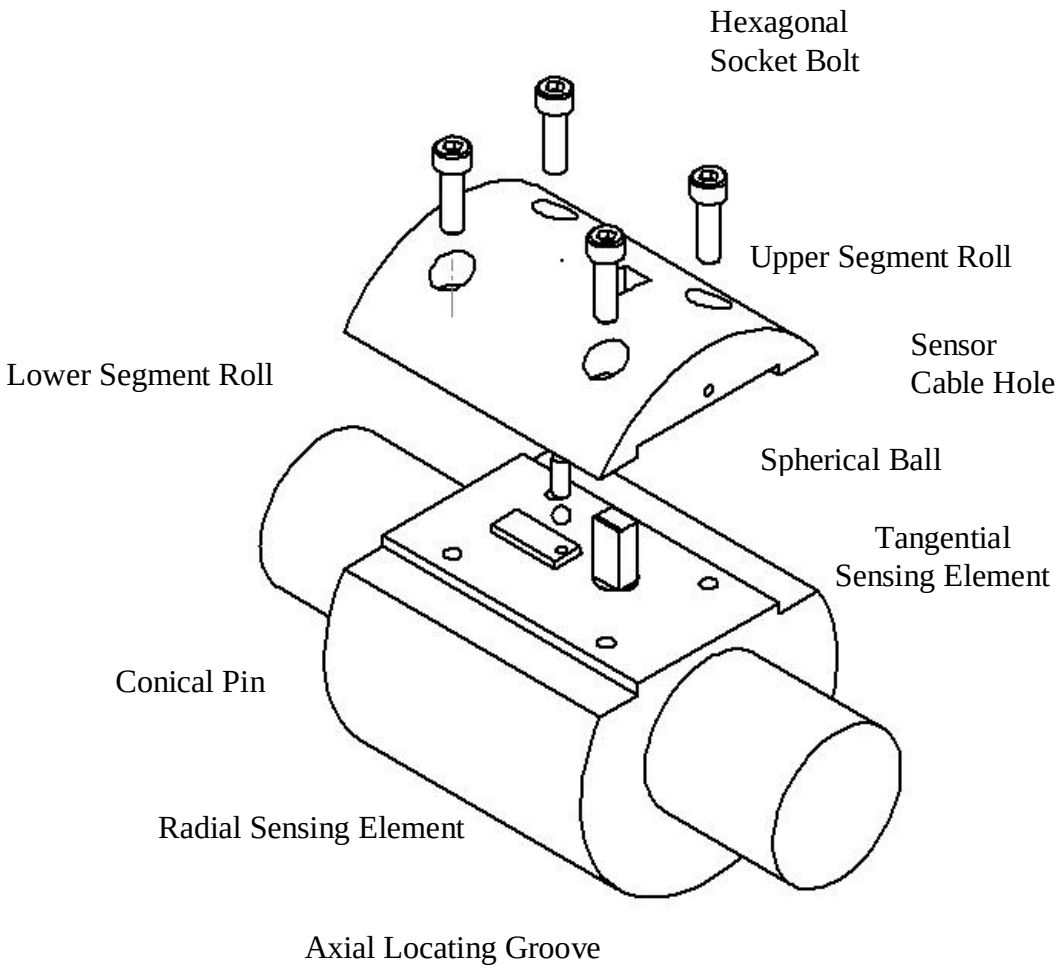

Figure 3.10. Exploded View of the SGRoll

3.2.1.2 Normal Pressure and Frictional Stress Measurement Principles

Figure 3.11 shows a schematic diagram of the radial sensing element. A conical pin was fitted radially into the sensor roll with the end flushing with the sensor roll surface, making contact with the work part during rolling operation. Consequently, the resulting normal force (F_R) was transmitted to the radial rectangular bar through the conical pin and the spherical ball. The transmitted normal force caused a strain in the radial rectangular bar which was measured with the strain gage. The output of the strain gage was sensed and picked up by the data acquisition system.

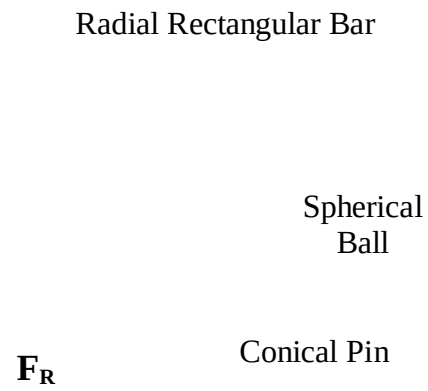

Figure 3.11. Normal Force Measurement Principle

Figure 3.12 shows a schematic representation of the tangential sensing element. A tangential rectangular bar which fitted radially into the SGRoll was located on the same axis as the conical pin, but a few inches apart. The end of the tangential rectangular

bar which flushed with the SGRoll surface made contact with the part during rolling. As the part was squeezed and pulled along the direction of the SGRoll, the frictional force (F_T) caused a strain in the tangential rectangular bar and was detected with the strain gage.

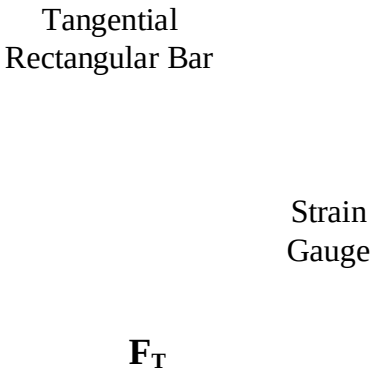

Figure 3.12. Frictional Force Measurement Principle

The strain gage was calibrated in order to convert strain output signals to equivalent force measurements (Appendix D). Since the rectangular bars have uniform cross sectional areas, and also the material property was the same for all the parts of the SGRoll, the frictional stress resulted in a proportional relationship between the strain gage voltage output and the stresses, the constant of proportionality being the conversion factor.

The material used in manufacturing the SGRoll is 4140 heat treated steel. Figure 3.13 is a photograph of the manufactured SGRoll. The performance of the SGRoll compares with other measuring techniques whose designs are much more sophisticated and costly.

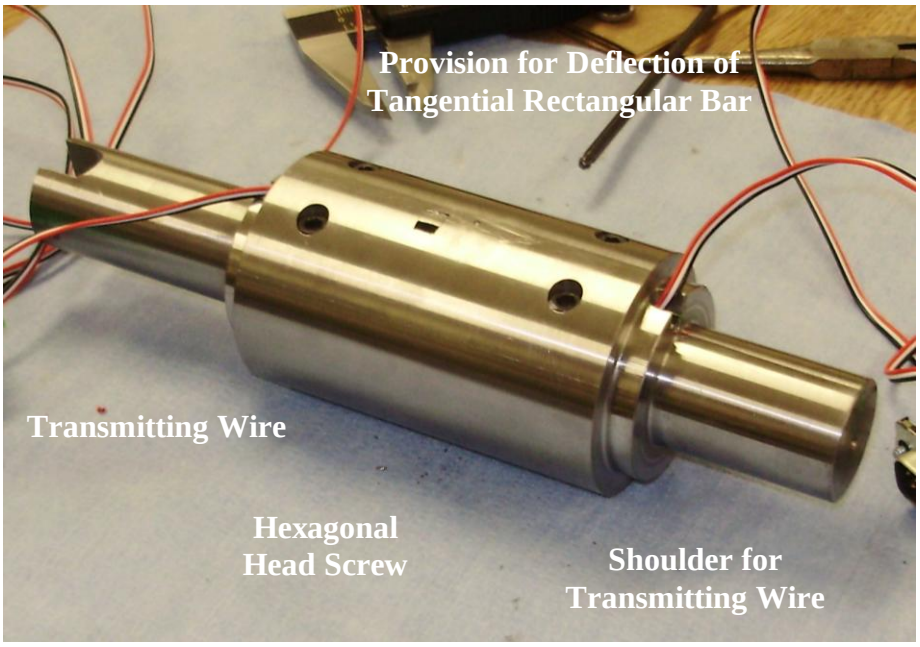

Figure 3.13. Photograph of the SGRoll

3.2.1.3 Experimental Work

Tests were carried out on a two-high experimental rolling mill powered by a variable speed motor of 0.5 horse power at the roll. The maximum rolling force and the rotational speed were 30,000 Ib and 20 rpm, respectively. The rolls were of dimensions 2 inch diameter and 4 inch length. The roll gap which controlled the exit thickness of the workpart was set using an adjustable screw system. The maximum available gap was 0.5

inches. The data acquisition system included System 5000 Scanner and Strain Smart Software. The System 5000 Scanner picked up signals through the transmitting wires while the Smart Strain Software processed the data. The sampling rate was 100 Hz. The strain gage transmitting wires from the SGRoll were connected to the input of the System 5000 Scanner. Figure 3.14 is a photograph of the experimental set up. During rolling, the SGRoll and the lower roll progressively squeezed the work part as the work part entered and exit the rolls. As a result, the conical pin caused a strain in the radial rectangular bar. Simultaneously, the tangential rectangular bar caused a strain in the tangential rectangular bar. The strain in the respective strain gages changed the output of the wheatstone bridge set up enclosed in the System 5000 Scanner.

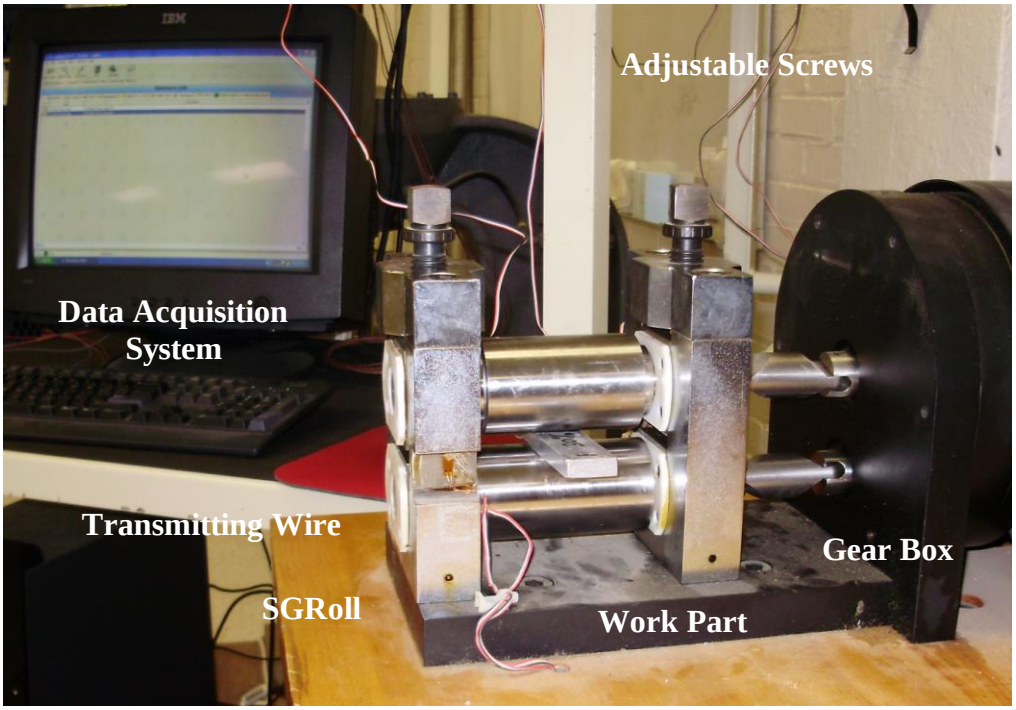

Figure 3.14. Photograph of Experimental Set Up

3.2.1.4 Experimental Procedure

Aluminium alloy 1100 with dimensions of 0.375-inch thick and 1-inch wide was used in the experiments. Design calculations (Appendix E) revealed that reductions below 30% was not feasible with the data acquisition system, for the maximum sampling rate of 100 Hz. Reductions above 30% was not successful in one pass rolling due to the roller speed. Consequently, the reduction was fixed at 30%. The experimental steps are as follows:

1. Cut the specimen to size and chamfer one end of specimen to facilitate entry into the rolls.
2. Set the roll gap to the exit thickness.
3. Turn on the main power to the control panel. Start hydraulic power unit and set speed to conform to the selected speed. In this experiment, the selected speed was 5 rpm.
4. Select FWD knob of the roll mill. Feed the specimen through the roll gap and select STOP knob of the roll mill. At this point ensure that the axis of the conical pin and tangential rectangular bar are well marked or located.
5. Check the SGRoll transmitting wire readings to ensure that there is no strain on the strain gage. Connect the transmitting wires to the input socket of the System 5000 Scanner. Once again check strain gage readings at the input socket. Turn ON System 5000 Scanner
6. Initiate Smart Strain software. Set the sampling rate. In this experiment, the sampling rate was set at 100 Hz. Match System 5000 Scanner input

channel to Smart Strain software channel. In this experiment, channel 1 is for the radial rectangular bar and channel 2 is for the tangential rectangular bar. Perform net zero strain and shunt calibration. At this point the data is ready to be collected.

7. Hit START on the recording pop up menu. Then select FWD knob of the roll mill. Rolling starts. As soon as the axis of the conical pin exits the contact region, hit STOP on the recording pop up menu, and then select STOP on the roll mill. Smart Strain software prepares the output file and presents it in Excel format.

The measured data from the experiment is shown in Table F1 (Appendix F) and also presented in Figure 3.15.

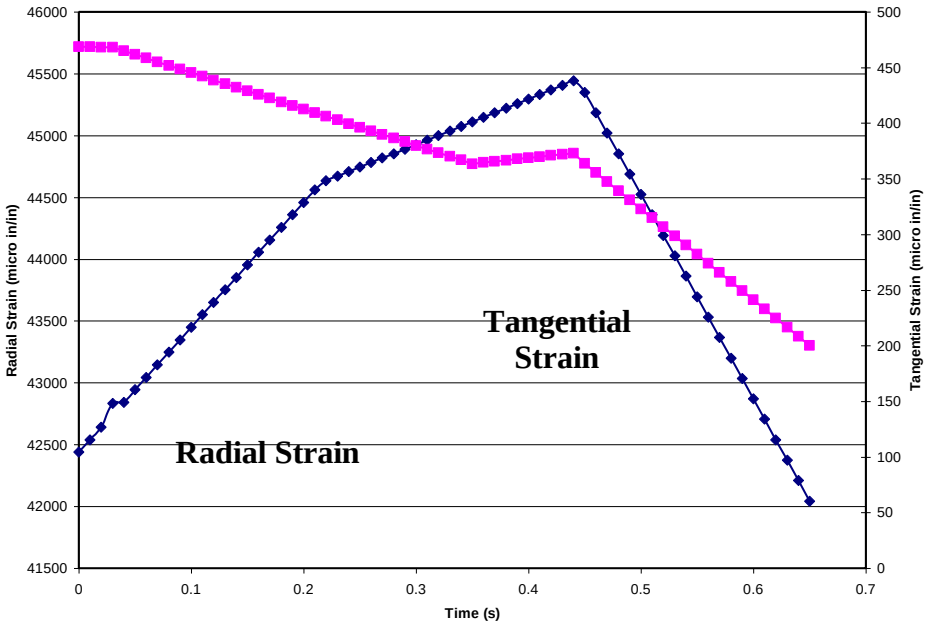

Figure 3.15. Plot of Measured Data

From Figure 3.15, friction and slipping between the work and roll interface caused the radial strain to increase continuously as work entered the roll until maximum radial strain is attained at a time of about 0.45 seconds. Thereafter, the friction and slipping between the work and roll interface caused the radial strain to decrease rapidly until the work exited the roll Also, the tangential strain decreased continuously as the work entered the roll until about half way through the contact region. The tangential strain remained stationary for a few seconds and thereafter decreased rapidly as the work part exited the roll. The next chapter discusses the extraction of the dynamic friction coefficient from the measured data and how it was used to develop the pressure distribution.

CHAPTER 4

ANALYSIS AND DISCUSSION OF RESULTS

The instantaneous coefficient of friction is derived from the experimental data and it is used to study its effects on the friction hill using the various modified models discussed in the previous chapter. Pressure distributions, frequently referred to as the friction hills, are also developed and discussed in this chapter.

4.1 Extraction and Analysis of Instantaneous Friction Coefficient

Table 4.1 shows the results obtained from the experiment. The raw data is presented in Table F2 of Appendix F. The normal force and frictional force was evaluated using the strain - force calibration charts. Subsequently, the friction coefficient was calculated as the ratio of frictional force to the normal force. The friction coefficient derived from the experiment is plotted in Figure 4.1.

Table 4.1. Extraction of Measured Friction Coefficient

Time (s)	θ (rad)	Strain - Force Calibration		μ
		Normal Force (lbf)	Friction Force (lbf)	
0.00	0.337	462	49	0.1062
0.05	0.311	468	48	0.1034
0.10	0.285	473	47	0.0986
0.15	0.259	479	45	0.0939
0.20	0.233	484	43	0.0893
0.25	0.207	487	42	0.0853
0.30	0.181	489	40	0.0814
0.35	0.155	491	38	0.0777

The plot indicates that as the part made contact with the roll, the friction coefficient decreased slowly from a maximum value of about 0.11 until the point of no-slip. At this point, the friction coefficient decreased rapidly as the work exited the roll. The position of the no-slip point was identified to be θ_{NS} = 0.13 radians from the exit point. The mathematical relationship between the friction coefficient and the roll angle was determined and the results are shown in Equations 4.1 and 4.2.

$$\mu_{Before} = -0.2105\theta^2 + 0.2087\theta + 0.0606 \tag{4.1}$$

$$\mu_{After} = 0.3077\theta + 0.0452 \tag{4.2}$$

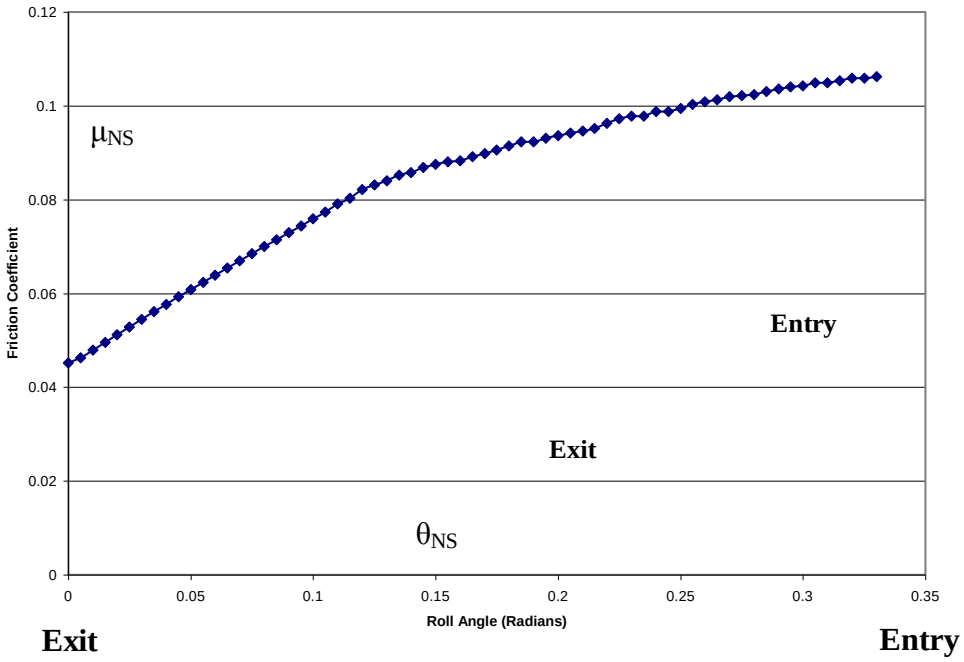

Figure 4.1. Measured Friction Coefficient

Comparison of the measured friction coefficient and the friction coefficient models were made and the result is presented in Figure 4.2. The modified Avitzur model and the experimental results revealed that, as the work part made contact with the roll, the friction coefficient decreased gradually from a maximum value until the no-slip point. Thereafter, the friction coefficient decreased rapidly as the work part exited the roll. The modified Tieu shows that friction coefficient decreased slowly until the no-slip point and becomes constant as the work part exited the roll. Thus the modified Avitzur model seemed to represent the accurate characteristics of the process since it compares favorably with the experimental results.

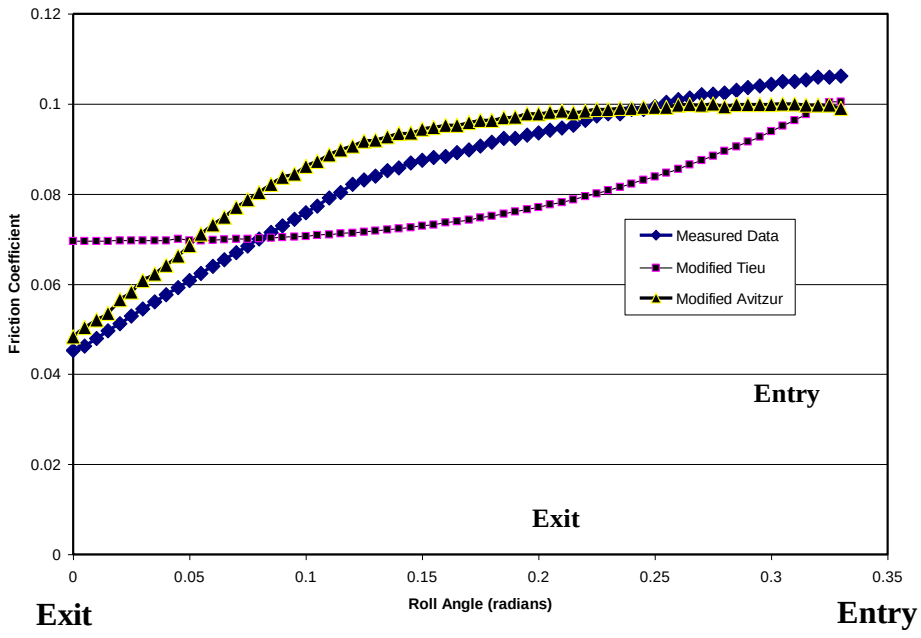

Figure 4.2. Comparison of Friction Coefficient Models with Experimental Data

4.2 Analysis of Pressure Distribution

Pressure distributions were analysed using the constant friction coefficient approach and the modified friction coefficient models. The constant friction coefficient models considered was the Rule of Thumb, Tieu model, and Avitzur model. The varying friction coefficient models considered were (1) Experimental, (2) modified Tieu model, and (3) modified Avitzur model.

4.2.1 Pressure Distribution for Constant Friction Coefficient

For rolling to be accomplished, the friction coefficient between the work and roll interface must be sufficient enough to overcome the roll resistance. Equation 4.3 provides the physical constraint of the process, where, μ and θ_{max} are friction coefficient and bite angle respectively.

$$\mu \geq \tan\theta_{max} \tag{4.3}$$

From Equation 4.3, and the input parameters of Tieu, the theoretical friction coefficient was evaluated to be a minimum of 0.085, while the rule of thumb friction coefficient is normally chosen as 0.1 for a cold-rolling operation.

From Equations 1.6, 1.7, 1.8, 1.9, and Matlab Program 3 in Appendix B, the variation of pressure distribution for a rule of thumb friction coefficient model ($\mu = 0.1$) is provided in Figure 4.3. Friction between the work and roll interface caused the pressure to increase exponentially as the work entered the rolls until the maximum pressure is attained at a location of about 0.026 radians from the exit point. Thereafter, the pressure decreased almost linearly until the work exited the roll.

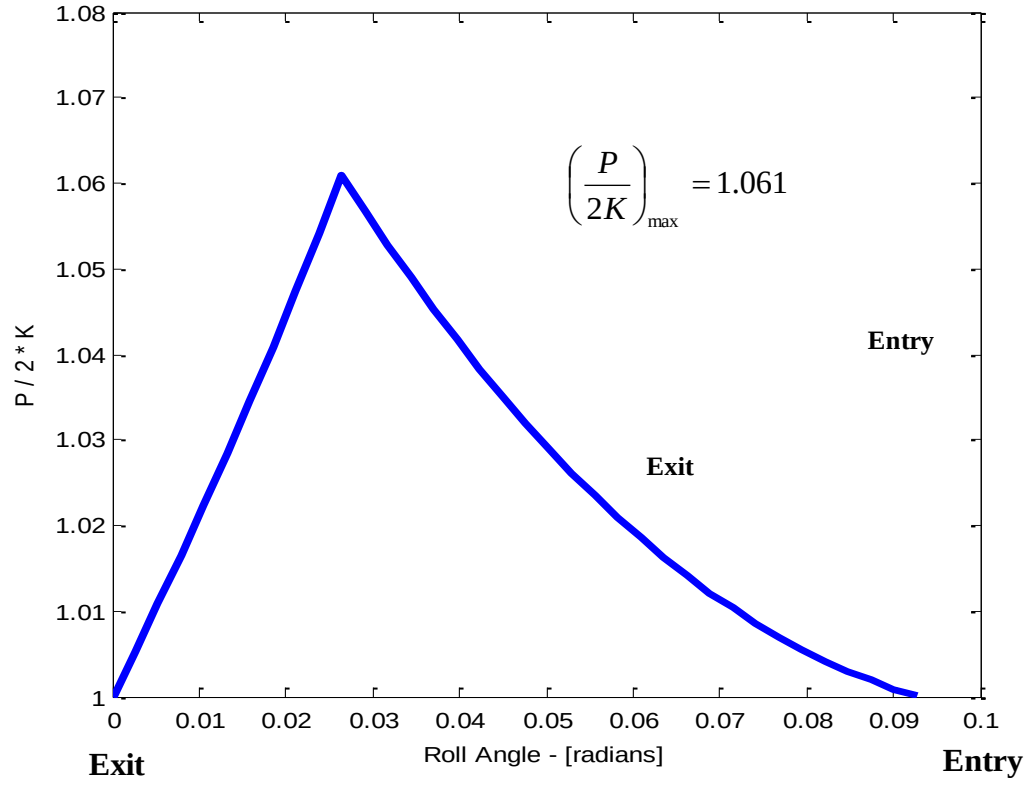

Figure 4.3. Variation of Pressure Distribution – Rule of Thumb

The coefficient of friction based on Tieu and Avitzur models were estimated using Equations 3.2 and 3.5, respectively and the variation of pressure distribution was determined and presented in Figures 4.4 and 4.5. The pressure distribution patterns for the three cases for the constant friction coefficient models were similar with minor differences in the peak pressures and their location.

Comparison of the three cases of constant friction coefficient models (Rule of Thumb, Tieu Model, and Avitzur Model) was made. The results are shown together in Figure 4.6. It can be seen that as the coefficient of friction increased, the no slip point

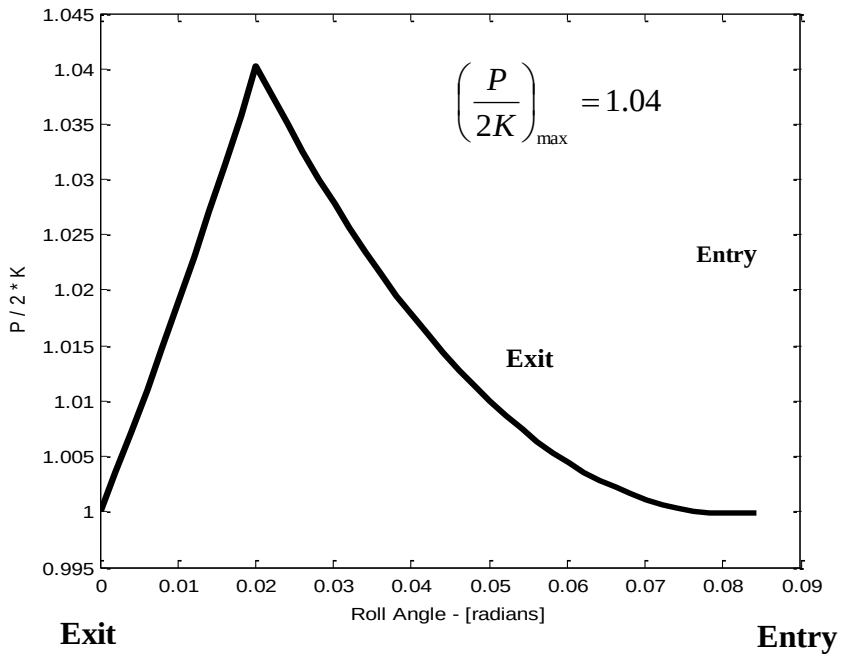

Figure 4.4. Variation of Pressure Distribution – Tieu

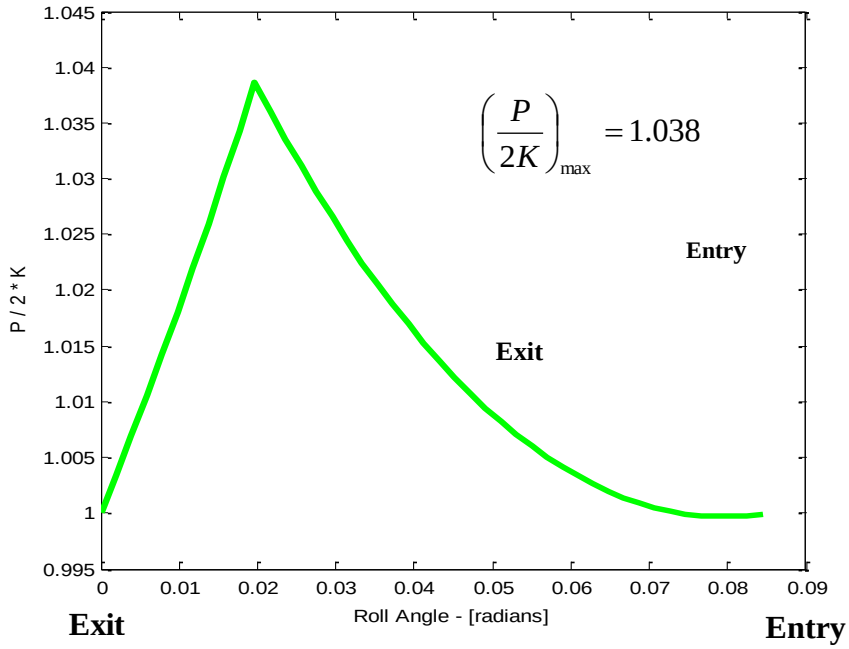

Figure 4.5. Variation of Pressure Distribution – Avitzur

shifted towards the entry, and the peak pressure increased. The area under the pressure distribution curves can be shown to be proportional to the power and force required for the rolling operation. Thus, as the friction coefficient increased, the power required in performing the operation increased. The detectable changes in the area under the pressure curves, peak pressures and the location of no-slip point compared with the small changes in friction coefficient values confirmed that the friction coefficient is a very sensitive parameter.

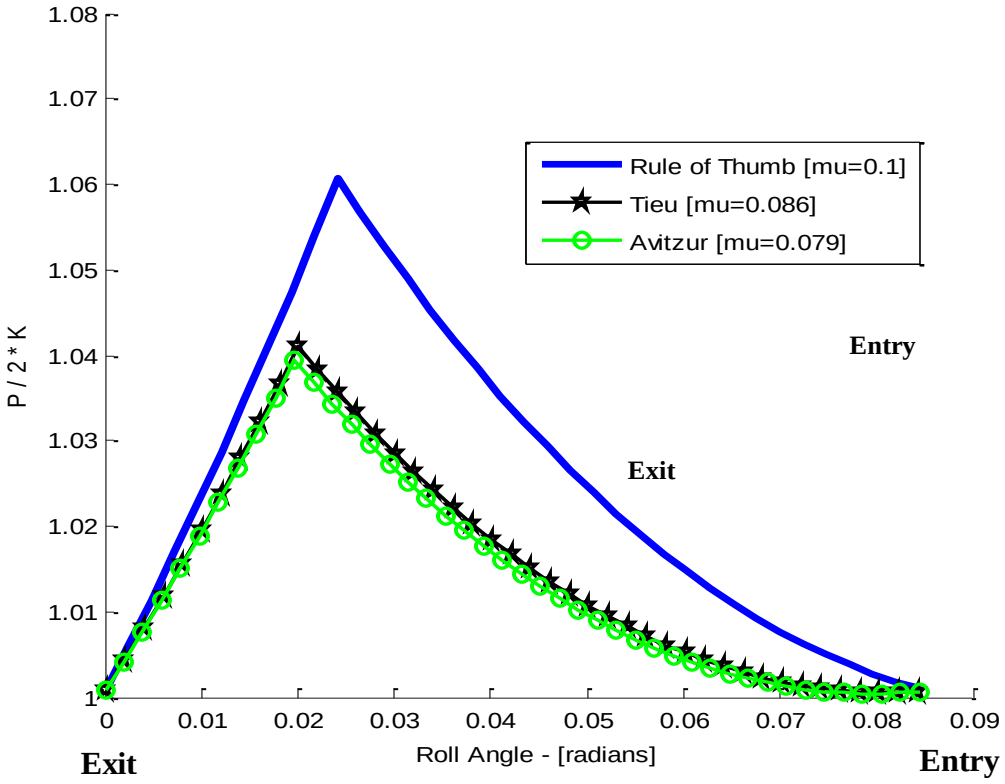

Figure 4.6. Comparison of Pressure Distribution – Constant Friction Models

Thus maximum care must be taken in its estimation. It can be said that the Rule of Thumb value which is used in industry leads to an over-estimation according to the Tieu and Avitzur models.

4.2.2 Pressure Distribution for Varying Friction Coefficient

Referring to Figure 1.7, the principal stresses are evaluated by considering the fact that the frictional stresses lead to non-negligible shear stresses. Let the principal stresses be σ_1, σ_2, and σ_3 respectively.

$$\sigma_1 = \sigma_{av} + \tau_{\max} \tag{4.4}$$

$$\sigma_3 = \sigma_{av} - \tau_{\max} \tag{4.5}$$

where $\sigma_{av} = \frac{\sigma_x - P}{2}$, and $\tau_{\max} = \left[\left(\sigma_x - \sigma_{av}\right)^2 + \left(\mu P\right)^2\right]^{\frac{1}{2}}$. Now, evaluating σ_x from the distortion energy criterion of yielding for plane strain condition, by substituting σ_{av} and R into Equations 4.4, 4.5, and then further substitution into Equation 1.3 results in the expression for σ_x, which is shown in Equation 4.6.

$$\sigma_x = 2\left[\left(\frac{\sigma_0}{2}\right)^2 - \left(\mu P\right)^2\right]^{\frac{1}{2}} - P \tag{4.6}$$

Assuming that the effect of strain hardening on the material is negligible and thus the flow stress (σ_0) is constant, and differentiating σ_x with respect to θ results in the expression shown in Equation 4.7.

$$\frac{\partial \sigma_x}{\partial \theta} = -P' + \frac{-2P\mu^2 P' - 2P^2 \mu\mu'}{\left[\left(\frac{\sigma_0}{2}\right) - (\mu P)^2\right]^{\frac{1}{2}}} \tag{4.7}$$

where $\sigma_0 = \frac{2}{\sqrt{3}}\sigma_y$, and σ_y is the yield strength of the material. Now, rewriting Von Karman's Equation (Equation 1.2) in another form results in the expression shown in Equation 4.8.

$$h\frac{\partial \sigma_x}{\partial \theta} + \sigma_x \frac{\partial h}{\partial \theta} = 2PR(\sin\theta \pm \mu\cos\theta) \tag{4.8}$$

Substitution of the expressions for $\frac{\partial \sigma_x}{\partial \theta}$ and σ_x into Equation 4.8 results in the expression shown in Equation 4.9.

$$-P'h - h\left[\frac{2P\mu^2 P' + 2P^2\mu\mu'}{\left[\left(\frac{\sigma_0}{2}\right)^2 - (\mu P)^2\right]^{\frac{1}{2}}}\right] + 2h'\left[\left(\frac{\sigma_0}{2}\right)^2 - (\mu P)^2\right]^{\frac{1}{2}} - h'P = 2PR(\sin\theta \pm \mu\cos\theta) \tag{4.9}$$

Making P' the subject of Equation 4.9, results in the expression shown in Equation 4.10, where the normal pressure (P) and friction coefficient (μ) are functions of roll angle (θ).

$$P' = \{2PR(\sin\theta \pm \mu\cos\theta)\left[\left(\frac{\sigma_0}{2}\right)^2 - (\mu P)^2\right]^{\frac{1}{2}} + 2P^2\mu\mu' h - 2h'\left[\left(\frac{\sigma_0}{2}\right)^2 - (\mu P)^2\right] +$$

$$h'P\left[\left(\frac{\sigma_0}{2}\right)^2 - (\mu P)^2\right]^{\frac{1}{2}}\} \div \{-\left\{h\left[\left(\frac{\sigma_0}{2}\right)^2 - (\mu P)^2\right]^{\frac{1}{2}} + 2P\mu^2 h\right\}\} \qquad (4.10)$$

Equation 4.10 is the expression derived for estimating the pressure distribution along the contact length when friction coefficient between the work and roll interface is not assumed to be constant. The complexity of Equation 4.10 makes it necessary to obtain a solution by numerical methods. Using finite forward difference method to further simplify Equation 4.10, results in Equations 4.11.

$$P_{i+1} - P_i = \{2P_iR(\sin\theta_i \pm \mu_i\cos\theta_i)\left[\left(\frac{\sigma_0}{2}\right)^2 - (\mu_i P_i)^2\right]^{\frac{1}{2}}\Delta\theta + 2P_i^2\mu_i(\mu_{i+1} - \mu_i)h_i -$$

$$2(h_{i+1} - h_i)\left[\left(\frac{\sigma_0}{2}\right)^2 - (\mu P)^2\right] + (h_{i+1} - h_i)P_i\left[\left(\frac{\sigma_0}{2}\right)^2 - (\mu P)^2\right]^{\frac{1}{2}}\}$$

$$\div \{h_i\left[\left(\frac{\sigma_0}{2}\right)^2 - (\mu P)^2\right]^{\frac{1}{2}} + 2P_i\mu_i^2 h_i\} \qquad (4.11)$$

The minus and plus (±) signs in equation 4.11 occur because the direction of the friction force changes at the no-slip point. The plus sign applies between exit point and the no-slip point, while the minus sign applies between the entrance and the no-slip point.

The measured friction coefficient is modeled and presented in Equations 4.1 and 4.2. Now, we illustrate the estimation of pressure distribution using the friction

coefficient obtained from the experiment. From Equations 4.1, 4.2, and 4.11 the variation of the pressure distribution for the experimental friction coefficient model is determined. This is shown in Figure 4.7.

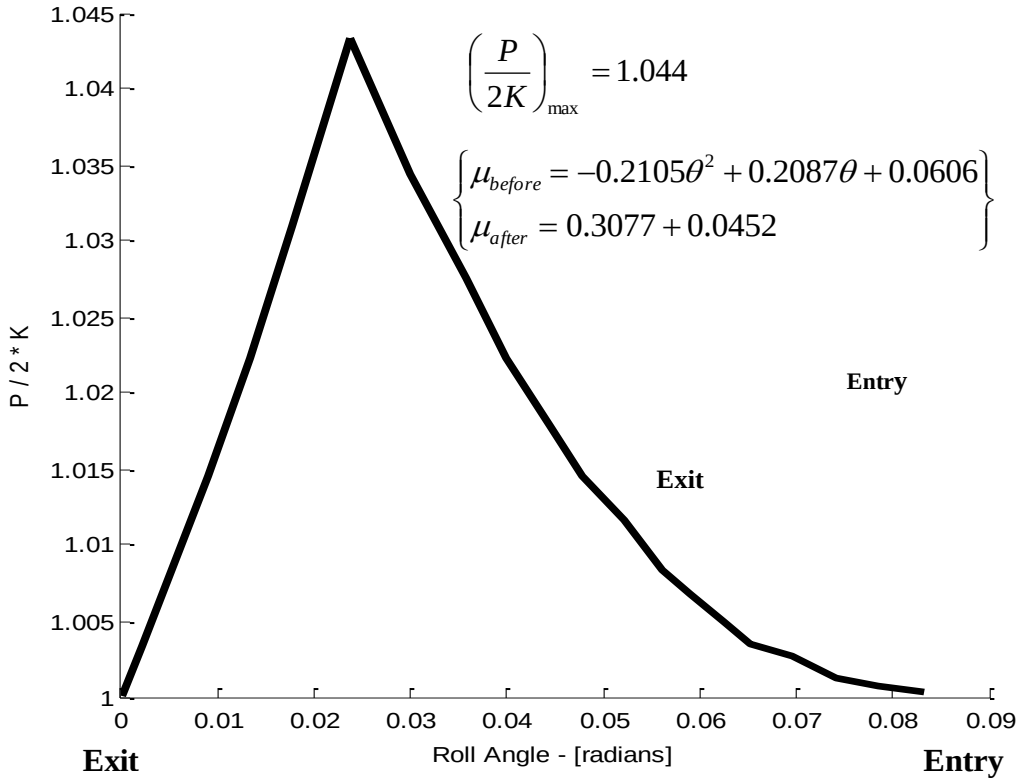

Figure 4.7. Variation of Pressure Distribution – Measured Data

From Figure 4.7, friction and slipping between the part and the roll interface caused the pressure to increase continuously as work entered the roll until a maximum pressure of $P/2K = 1.044$ was attained at the no-slip point estimated to 0.023 radians from the exit point. A comparison of Figure 4.3 shows that the no-slip points has shifted

slightly toward the exit and the peak pressure is lower than the constant value method. Similarly, the pressure distributions for the Modified Tieu and the Modified Avitzur friction coefficient models were also determined. This time Equations 3.8, 3.9, 3.11, 3.12 and 4.12 were used. The variation of pressure distribution for the Modified Tieu and Avitzur friction coefficient models are shown in Figures 4.8 and 4.9 respectively.

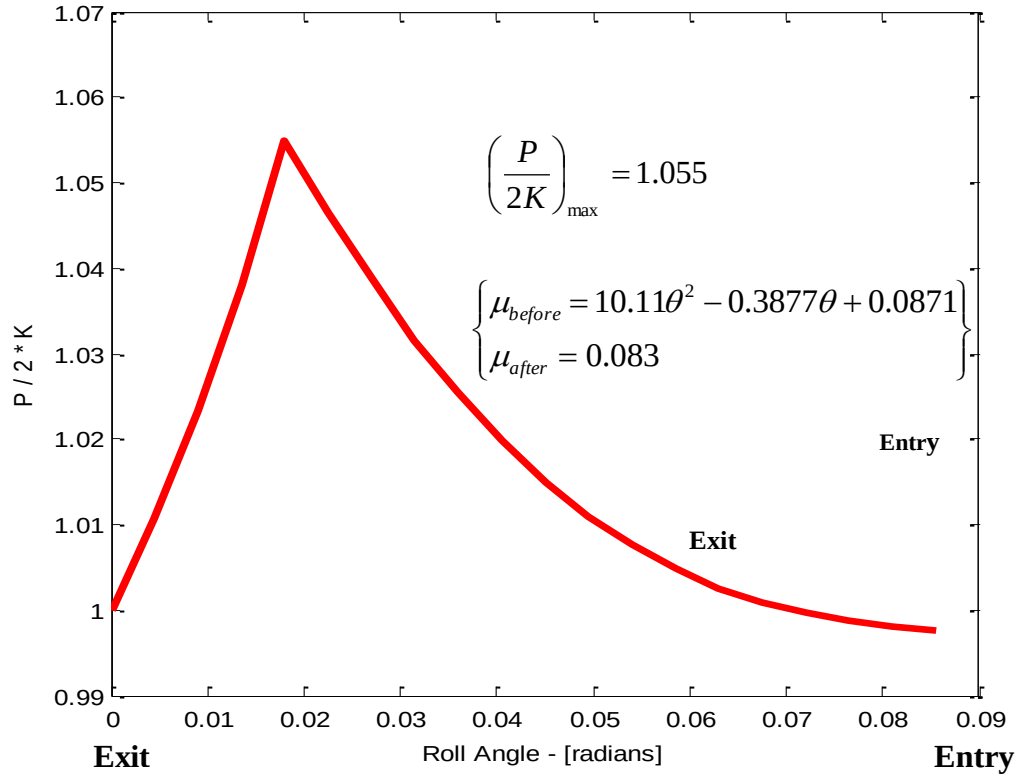

Figure 4.8. Variation of Pressure Distribution – Modified Tieu Model

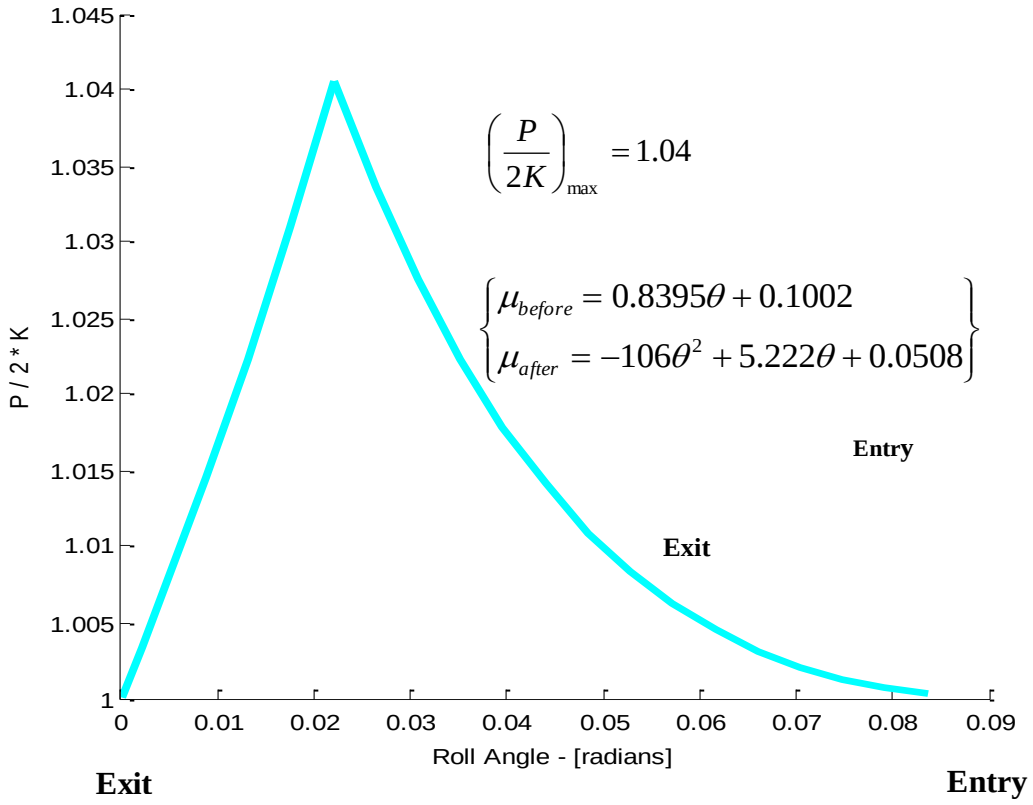

Figure 4.9. Variation of Pressure Distribution – Modified Avitzur Model

A comparison of the varying friction coefficient models (Measured, Modified Tieu Model, and Modified Avitzur) was made. The result is shown in Figure 4.10. The varying friction coefficient models showed the same trend and the same shape. The peak pressure for the modified Tieu model was higher than the peak pressures of the modified Avitzur and the measured. The power required for the rolling operation is proportional to the area under the pressure distribution curve. For the same parameters, Tieu's modified model would estimate the highest power requirement.

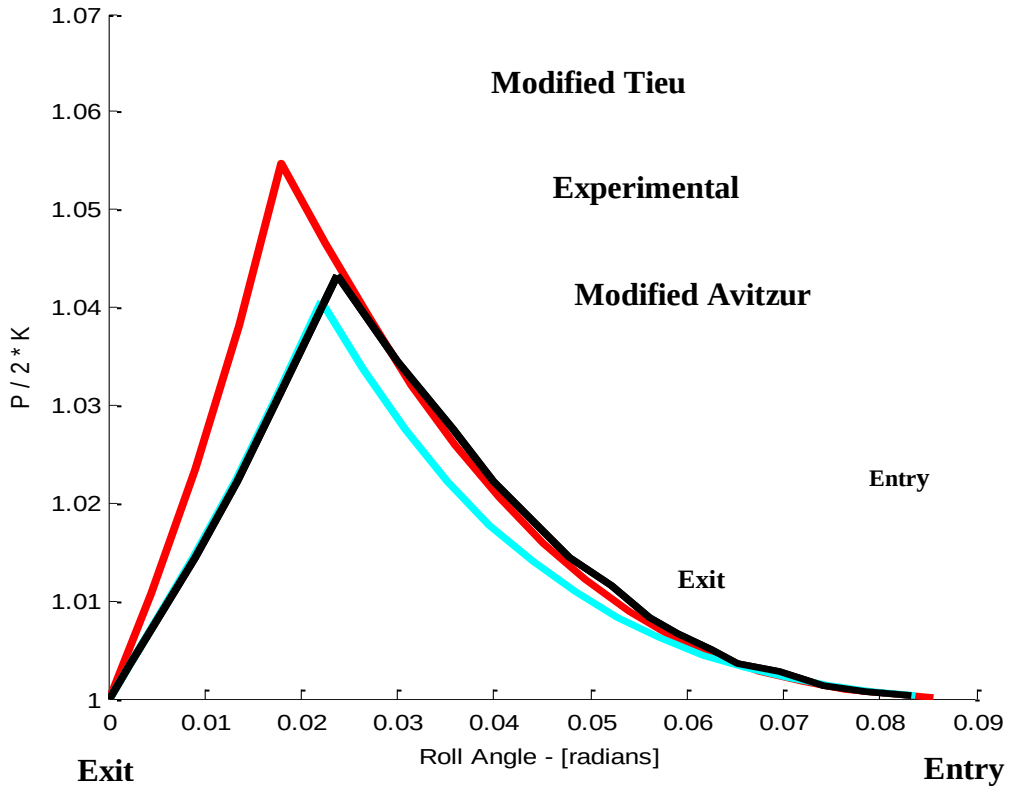

Figure 4.10. Comparison of Pressure Distribution – Modified Models and Experimental Data

A comparison of Rule of Thumb, Tieu, Avitzur, Measured, Modified Tieu Model, and Modified Avitzur Model was made. The results are shown in Figure 4.11. From Figure 4.11, as the coefficient of friction varied; (1) peak pressure changed, (2) area under the pressure distribution curve changed, and (3) the no-slip point shifted. Comparing each model with the experimental results suggests that, the rule of thumb model over-estimates the power requirements while Tieu and Avitzur's models under-estimate the power.

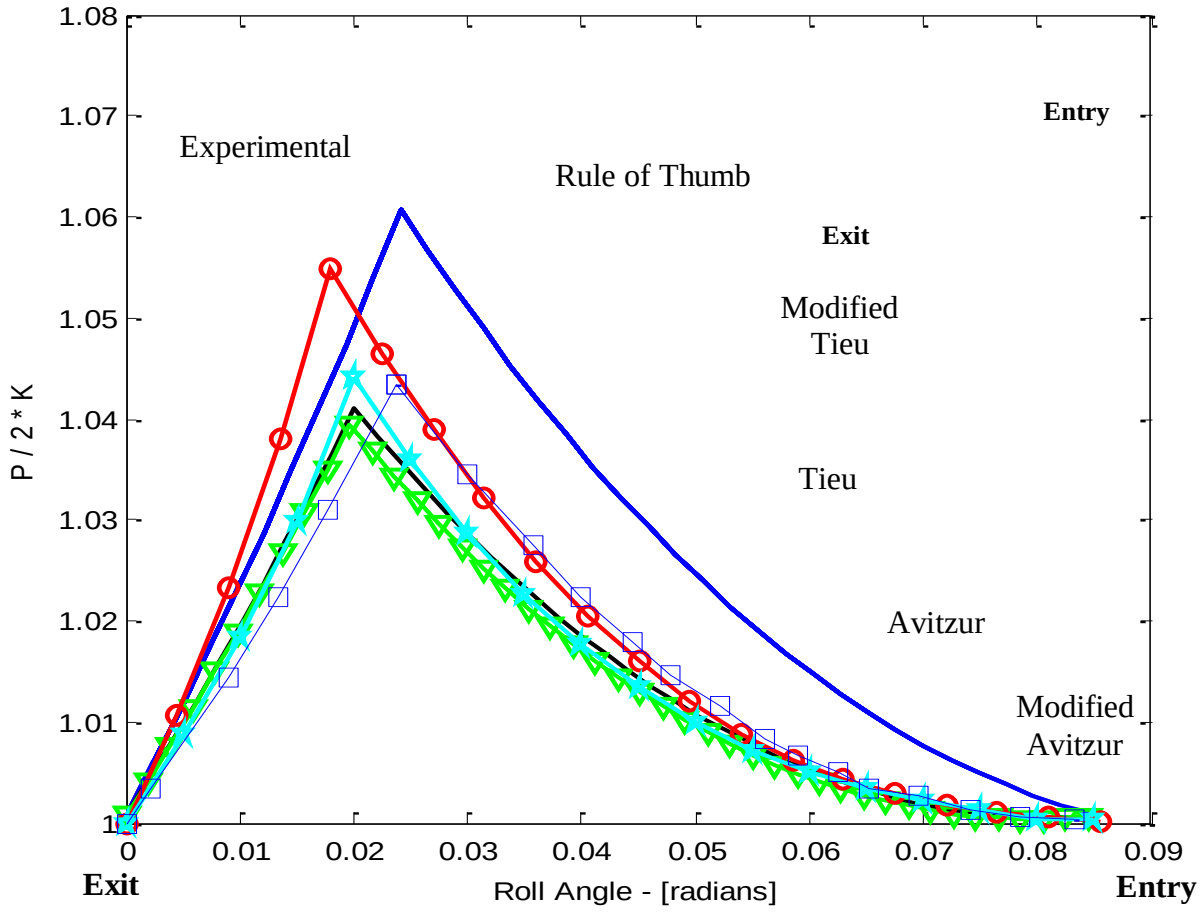

Figure 4.11. Comparison of Pressure Distribution for the Various Models

The under estimated parameters are undesirable in the cold rolling operation because of the following reasons: (1) cold rolling is a finishing operation in metal forming and the product quality could be highly compromised and (2) the life of the rolling equipment may be shortened due to high stresses.

Table 4.2 provides a numerical comparison of the parameters of the pressure distribution. It can be seen that the measured parameters compare most favorably with the Modified Avitzur Model. Their no-slip points are similar, the peak points are essentially equal in magnitude. The area under the curve are close to each other. Their savings in power compared to the rule of thumb model are almost the same. The Modified Avitzur Model resulted in 18% savings in power compared to the rule of thumb model while the Modified Tieu Model resulted in 16% savings. Avitzur and Tieu's original models suggest 26% and 22% savings in power respectively compared to the rule of thumb model. This savings suggest lesser deformation forces which could be a concern with respect to the dimensional accuracy and precision of the product.

4.3 Effect of Strain Hardening on Pressure Distribution

In this analysis, an allowance is made for the fact that the flow stress (σ_0) changes with respect to the roll bite angle (θ) due to strain hardening. Using Equation 4.6 and differentiating σ_x with respect to θ results in Equation 4.12.

$$\frac{\partial \sigma_x}{\partial \theta} = -P' + \frac{-2P\mu^2 P' + \frac{1}{2}\sigma_0 \sigma_0' - 2P^2 \mu\mu'}{\left[\left(\frac{\sigma_0}{2}\right) - (\mu P)^2\right]^{\frac{1}{2}}} \tag{4.12}$$

Table 4.2. Comparison of Pressure Distribution Parameters for the Various Models

Parameter	Friction Coefficient Models					
	Current Approach			Based on this Research		
	Rule of Thumb	Tieu	Avitzur	Modified Tieu	Modified Avitzur	Experimental
Theta Neutral (θ_N) - Radians	0.0241	0.0201	0.0196	0.0189	0.022	0.023
Peak - (P / 2*K)	1.061	1.041	1.039	1.055	1.04	1.044
Area (A) – unit^2	0.1429	0.1122	0.1053	0.1196	0.1167	0.1159
Percentage Change in Area (A %)	0	-21.48	-26.31	-16.31	-18.33	-18.89

Substituting Equations 4.13 and 4.6 into Equation 4.8 results in the expression shown in Equation 4.14.

$$-P'h-h\left[\frac{2P\mu^2P'-\frac{1}{2}\sigma_0\sigma_0'+2P^2\mu\mu'}{\left[\left(\frac{\sigma_0}{2}\right)^2-(\mu P)^2\right]^{\frac{1}{2}}}\right]+2h'\left[\left(\frac{\sigma_0}{2}\right)^2-(\mu P)^2\right]^{\frac{1}{2}}-h'P=$$

$$2PR(\sin\theta\pm\mu\cos\theta) \qquad (4.13)$$

Further simplification of Equation 4.13 results in Equation 4.14. Equation 4.14 is the expression for estimating the pressure distribution of rolling operation with strain hardening as a function of the roll angle. Once again, the complexity of Equation 4.14 makes it necessary to obtain solution by numerical methods. Using finite forward difference method to simplify Equation 4.14, results in Equations 4.15.

$$P'=\{2PR(\sin\theta\pm\mu\cos\theta)\left[\left(\frac{\sigma_0}{2}\right)^2-(\mu P)^2\right]^{\frac{1}{2}}+2P^2\mu\mu'h-2h'\left[\left(\frac{\sigma_0}{2}\right)^2-(\mu P)^2\right]-$$

$$\frac{h}{2}\sigma_0\sigma_0^{'}+h'P\left[\left(\frac{\sigma_0}{2}\right)^2-(\mu P)^2\right]^{\frac{1}{2}}\}\div\{-\left\{h\left[\left(\frac{\sigma_0}{2}\right)^2-(\mu P)^2\right]^{\frac{1}{2}}+2P\mu^2h\right\}\} \qquad (4.14)$$

Next, we estimate the pressure distribution within the contact region using Equations 4.15 and the modified friction coefficient models.

The variation of pressure distribution within the contact region for the Modified Tieu and Avitzur Models were estimated. Equations 3.8, 3.9, 4.15 were used to evaluate

$$P_{i+1} - P_i = \{2P_i R(\sin\theta_i \pm \mu_i \cos\theta_i)\left[\left(\frac{\sigma_0}{2}\right)^2 - (\mu_i P_i)^2\right]^{\frac{1}{2}} \Delta\theta + 2P_i^2 \mu_i(\mu_{i+1} - \mu_i)h_i -$$

$$\frac{h_i}{2}\sigma_{0i}(\sigma_{0i+1} - \sigma_{0i}) - 2(h_{i+1} - h_i)\left[\left(\frac{\sigma_0}{2}\right)^2 - (\mu P)^2\right] + (h_{i+1} - h_i)P_i\left[\left(\frac{\sigma_0}{2}\right)^2 - (\mu P)^2\right]^{\frac{1}{2}}\} \div$$

$$\{h_i\left[\left(\frac{\sigma_0}{2}\right)^2 - (\mu P)^2\right]^{\frac{1}{2}} + 2P_i\mu_i{}^2 h_i\} \qquad (4.15)$$

pressure distribution for the Modified Tieu Model. The result is shown in Figure 4.12. Similarly, equations 3.11, 3.12, 4.15 were used to evaluate the pressure distribution for the Modified Avitzur Model. The result is shown in Figure 4.13. Both results indicated that the pressure increased continuously as work entered the roll until maximum pressure was attained at a location equal to the no slip point of about 0.02 radians from the exit point. Thereafter, pressure decreased rapidly from the no slip point until the work exited the roll. The pattern of the pressure distribution suggests that as the material undergoes strain hardening, more power was required as rolling progressed.

A comparison of the estimated pressure distributions with and without strain hardening effects was made for the Modified Avitzur and Tieu Models. The results are presented in Figures 4.14 and 4.15. It was observed that strain hardening effects: (1) increased the magnitude of the roll pressure, (2) increased the peak pressure, (3) shifted the no-slip point closer to the exit point in relation to the modified Avitzur model, and (4) shifted the no-slip point closer to the entry point in relation to the modified Tieu model.

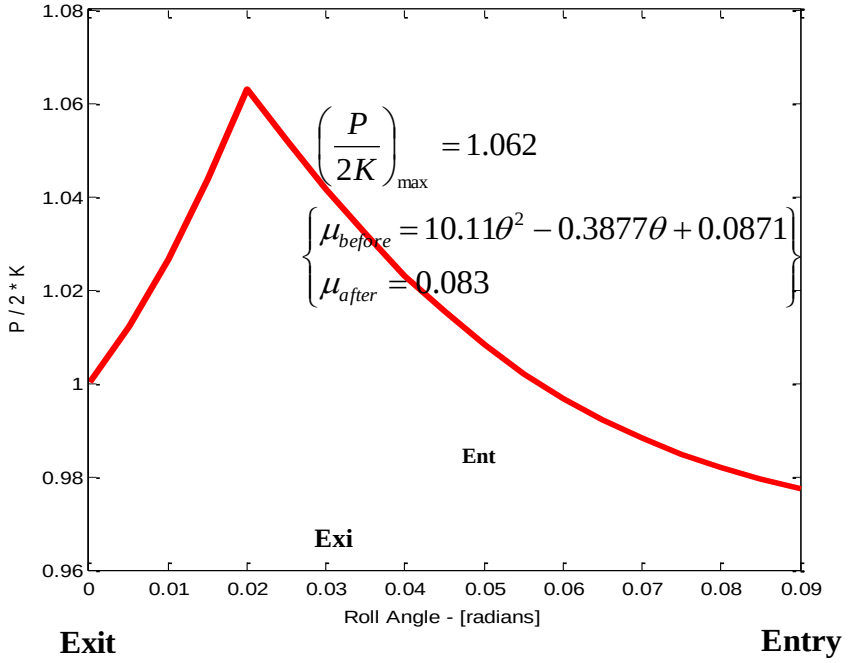

Figure 4.12. Strain Hardening Effects – Modified Tieu Model

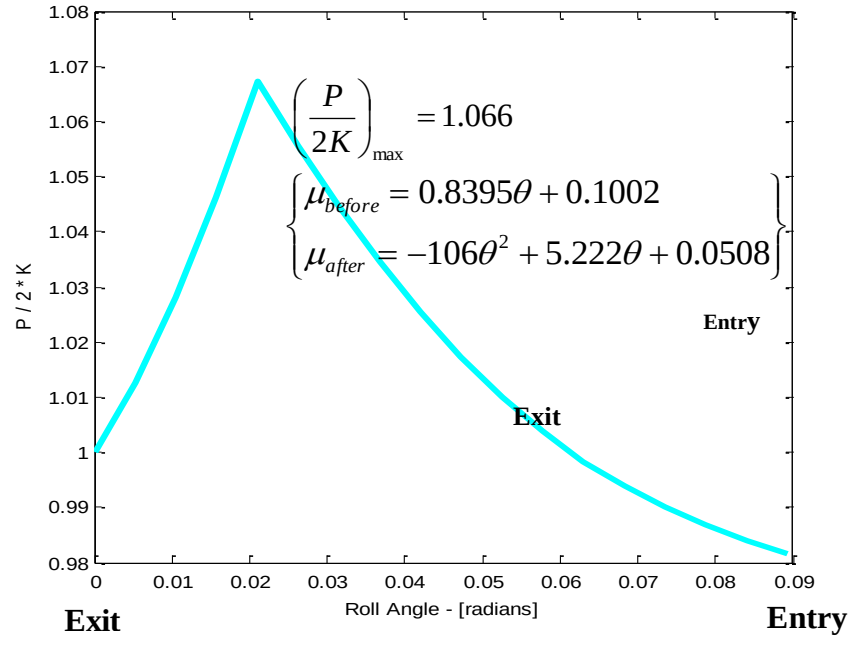

Figure 4.13. Strain Hardening Effects – Modified Avitzur Model

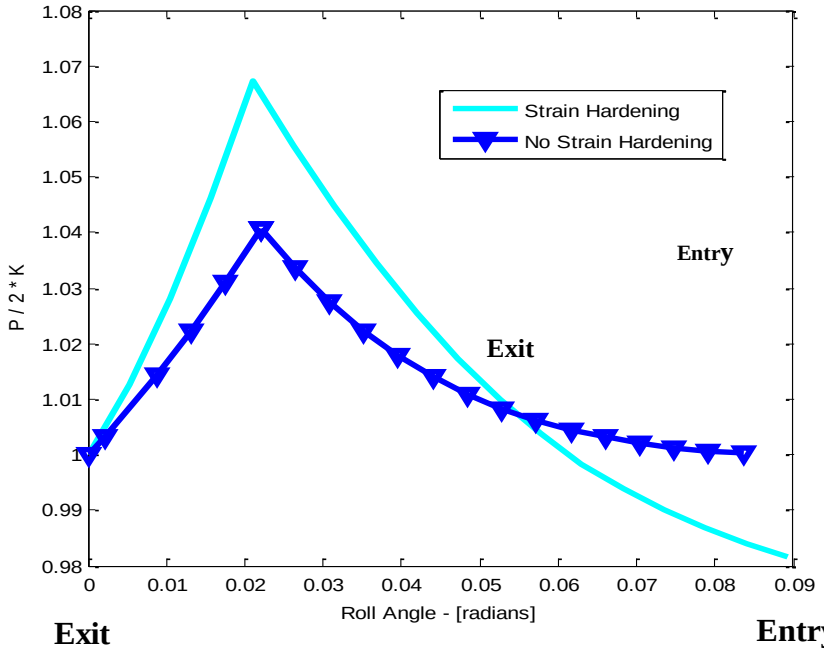

Figure 4.14. Comparison of Pressure Distribution – Modified Avitzur Model

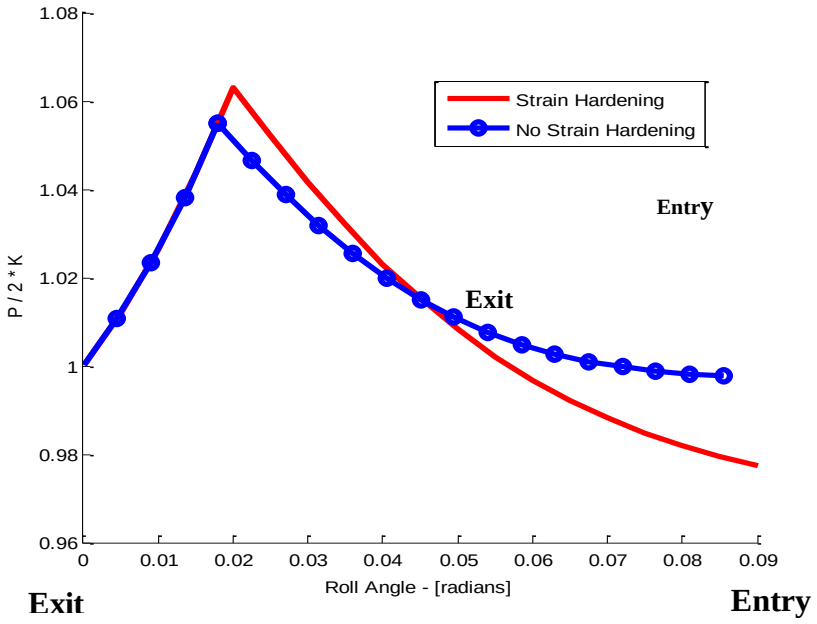

Figure 4.15. Comparison of Pressure Distribution – Modified Tieu Model

CHAPTER 5

CONCLUSIONS AND RECOMMENDATIONS

A quantitative relationship between the friction coefficient and the incremental roll angle within the contact region of a cylindrical element on flat surface has been determined. Two of the current friction coefficient models which give constant coefficient of friction values have been modified to yield varying values which are consistent with the physics of the process. The utilization of the relationship between the friction coefficient and roll angle, and the modified models has improved the accuracy of the estimation of the pressure distribution during the rolling operation. In order to validate the mathematical relationship between the friction coefficient and the roll angle, a simple friction coefficient measurement technique has been developed and tested. This measurement technique and the modified pressure distribution models developed could complement the efforts of the industry in predicting the power and energy requirements for the process.

5.1 Conclusions

Pressure distribution models have been developed within the contact region using a varying friction coefficient model. The following specific conclusions may be drawn from the results obtained in the work.

1. Current industrial practices overestimate the pressures required for the rolling operation. Though this ensures a permanent deformation, it could lead to poor product quality such as cracking.
2. A classical method proposed by Avitzur and an empirical method proposed by Tieu in attempts to improve upon the prediction of the rolling pressure tend to underestimate the pressure distribution from the entry to the no-slip point and overestimate it from the no-slip point to the exit point.
3. There is 16% to 18% savings in the rolling power requirement using the varying coefficient of friction modeling techniques over the traditional constant coefficient of friction method.
4. The strain hardening effect increases the magnitude of the peak pressure within the contact zone as well as the power requirement.

The following observations can be made from the results of the friction coefficient measuring technique developed.

1. The friction coefficient decreases from the entry point to the exit point, which is consistent with the physics in the contact region.
2. The experimental friction coefficient values compare favorably with those obtained from the modified Avitzur model developed through this study.
3. The pressure distribution resulting from the experimental friction coefficient model compares favorably with the modified Tieu model between the entry

and the no-slip points and compares favorably with the modified Avitzur model between the no-slip and the exit points.

5.2 Recommendations

The following recommendations are offered from the results.

1. The experimental setup may be improved by extending the angles of rotation of the roll. The transmitting wires used in the experiment had the tendency of limiting the number of angular rotations. Further design work needs to be done to extend the range of the data collected. This may include the use of a wireless SGRoll.
2. The relationship between the friction coefficient and roll angle should be further investigated for different types of materials and reduction ratios. A reduction of 30% was used in this experiment with a specific roll diameter and material properties.
3. The quantitative relationship between the friction coefficient and roll angle should be utilized in designing a rolling software for the accurate evaluation of the rolling parameters.

The results of this work allows the scientific and the engineering world to realize the importance of applying instantaneous value of the coefficient of friction in the evaluation of the characteristics of the pressures in the contact region during the plastic deformation of a metallic slab. Through this work, the power and energy requirements are determined more accurately than the present methodologies.

REFERENCES

Abdollahi H., and Dehghani, K., (2007), "Study of Friction Distribution during the Cold Rolling of Materials by Matroll," *10th ESAFORM Conference on Material forming, AIP Conference Proceedings*, Vol. 907, pp. 547-551.

Abdollahi H., and Dehghani, K., (2008), "Irregularities in Friction Hills during Cold Rolling of Materials," *International Journal of Material Forming*, Vol. 1, Suppl. 1, pp. 343-346.

Al-Salehi, F. A. R., Firbank, T. C., and Lancaster, P. R., (1973), "An Experimental Determination of the Roll Pressure Distribution in Cold Rolling," *International Journal of Mechanical Science*, Vol. 15, pp. 693-710.

Avitzur, B., (1964), "An Upper-Bound Approach to Cold-Strip Rolling," *Transactions of American Society of Mechanical Engineers, Series B*, Vol. 86, pp. 31-48.

Avitzur B., *Metal Forming, Process and Analysis*, McGraw-Hill Book Company, New York, 1968, pp 475-476.

Avitzur B., *Metal Forming, The Application of Limits Analysis*, Marcel Dekkler Inc., New York, 1980, pp. 55-57.

Beddoes J. and Bibbey M. J., *Principles of Metal Manufacturing Processes*, John Wiley & Sons Inc., New York, 1999, pp. 127.

Bland, D. R. and Ford, H., (1948), "The Calculation of Roll Force and Torque in Cold Strip Rolling with Tensions," *Proceedings for Institute of Mechanical Engineers*, Vol. 159, pp. 144.

Brown, C. M., *The Rolling of Metals, Theory and Experiment*, Chapman and Hall, London, 1950, pp. 164-166.

Dieter G. E., *Mechanical Metallurgy, Materials Science and Engineering Series*, McGraw-Hill Book Company, New York, Second Edition, 1976, pp. 613-614.

Doyle L. E., *Manufacturing Processes and Materials for Engineers, Third Edition*, Prentice-Hall Inc., New Jersey, 1985, pp. 253-255.

Fleck, N. A., Johnson, K. L., Mear, M., and Zhang, L. C., (1998), "Cold Rolling of Foil," Proceedings for Institute of Mechanical Engineers Part B: *Journal of Engineering Manufacture*, Vol. 206, pp. 119-131.

Gao H., Ramalingam S.C., Barber G.C., Chen G., (2002), "Analysis of asymmetrical cold rolling with varying coefficients of friction," *Journal of Materials Processing Technology*, Vol. 124, pp. 178-182.

Gelin J.C. and Ghouati, O., (1995), "Inverse Identification Methods for Material Parameters Estimation in Large Plastic Deformation," *Proceedings of COMPLAS*. 4th Edition, pp. 767-778.

Gosh, A. and Mallik, A. K., *Manufacturing Science*, Ellis Horwood Limited, Chichester, 1986, pp. 112-115.

Groover M. P., *Fundamentals of modern manufacturing materials, processes and systems*, John Willy & Sons Inc., New York, 1999, pp. 633-634.

Hill, R., (1963), "A General Method of Analysis for Metal Working Processes," *Journal of Physical Solids*, Vol.11, pp. 305-326.

Jeswiet J., (1995), "Aspect Ratio, Friction Forces and Normal Forces in Strip Rolling," *Journal of Materials Processing Technology*, Vol. 53, pp. 846-856.

Jeswiet, J. and Nyahumwa, C., (1993), "A Sensor for Measuring Metal Deformation Interface Forces," *Journal of Materials Processing Technology*, Vol. 39, pp. 251-268.

Jiang Z.Y. and Tieu A.K., (2004), "A 3-D Finite Element Method Analysis of Cold Rolling of Thin Strip with Friction Variation," *Tribology International*. Vol. 37, pp. 185-191.

Jiang Z.Y., Tieu A.K., Zhang X.M., Lu, C., and Sun, W.H., (2003), "Finite Element Simulation of Cold Rolling of Thin Strip," *Journal of Materials Processing Technology*. Vol. 140, pp. 542-547.

Keife H. and Sjogren C., (1994), "A Friction Model Applied in the Cold Rolling of Aluminum Strips," *Wear*, Vol. 60, pp. 137-142.

Kobayashi S., and Li G.J., (1982), "Rigid-Plastic Finite Element Analysis of Plane strain Rolling," *Journal of Engineering & Industry*, Vol.104, pp.55-64.

Kumar, M. D., Ramji, K., and Balasubrahmanyam, V. V., (2005), "Analysis of Strip Rolling using Finite Element Method and Numerical Integration Techniques," *Journal of Engineering & Industry*, Vol.85, pp.55-64.

Kurt L., *Handbook of Metal Forming*, Society of Manufacturing Engineers, United States of America, 1985, pp 12.1-12.9.

Lagergren, J., (1997), "Friction Evaluation in Hot Strip Rolling by Direct Measurement in the roll Gap of a Model duo Mill," *Journal of Material Processing and technology*, Vol. 70, pp. 207-214.

Lahoti G.D., Akgerman, N., Oh, S.I., and Altan, T., (1979), "Computer-Aided Analysis of Metal Flow and Stresses in Plate Rolling," *Journal of Mechanical Working Technology*, Vol.4, pp. 105-l19.

Larkiolda J., Myllykoski P., Nylander J.,and Korhonen, A.S., (1996), "Prediction of Rolling Force in Cold Rolling by using Physical Models and Neural Computing," *Journal of Materials Processing Technology*, Vol. 60, pp. 381-386.

Lau, C. W., Shivpuri, R., and Chou, P. C., (1987), "An Explicit Time Integration Elastic-Plastic Finite Element Algorithm for Analysis of High Speed Rolling," Submitted for publication to International Journal of Machining Science.

Le H.R. and Sutcli!e M.P.F., (2001), "A Robust Model for Rolling of Thin Strip and Foil," *International Journal of Mechanical Sciences*, Vol. 43, pp. 1405-1419.

Lenard, J. G., and Malinowski, Z., (1993), "Measurement of Friction during Warm Rolling of Aluminium," *Journal of Materials Processing Technology*, Vol. 39, pp. 357-371.

Lenard J. G., *Material Forming Science and Practice*, Elsevier Science Ltd., New York, 2002, pp. 90-91.

Lenard, J. G., (2004), "The Effect of Roll Roughness on the Rolling Parameters during Cold Rolling of an Aluminum Alloy," *Journal of Materials Processing Technology*, Vol. 152, pp. 144-153.

Lin, Z. C., and Lin, V. H., (1995), "Analysis of the Variation of the Cold-Rolling Characteristics of Rolling Force, Strip Shape, Stress and Temperature, for a Three-Dimensional Strip," *The Journal of Strain Analysis for Engineering Design*, Vol. 29, No. 4, pp. 267-276.

Liu X. H., Shi X., Li S. Q., Xu J. Y., Wang G. D., (2007), "FEM Analysis of Rolling Pressure along Strip Width in Cold Rolling Process," *Journal of Iron & Steel Research International*, Vol. 14 (5), pp. 22-26.

Liu, Y. J., Tieu, A. K., Wang, D. D., Yuen, W.Y.D., (2001), "Friction Measurement in Cold Rolling," *Journal of Materials Processing Technology*, Vol. 111, pp. 142-145.

Matlab (2007), The Mathworks Inc., Version 7.1.0.246 (R 14) Service Pack 3.

Orowan E., (1943), "The Calculation of Roll Pressure in Hot and Cold Rolling," *Proceedings for Institute of Mechanical Engineers*, Vol. 150, No. 4, pp. 140-167.

Roberts, C. D., (1997), "Mechanical Principles of Rolling," *Journal of Iron and Steel*, Vol. 24, pp. 113-114.

Rooyen, G. T. V. and Bachofen, W. A., (1957), "Friction in Cold Rolling," *Journal of the Iron and Steel Institute*, Vol. 6, pp. 235-244.

Sargent L. B., (1975), "Lubricants for Cold Rolling Aluminum Alloys – A Laboratory Appraisal," Light Metal Age, pp. 15-17.

Siebel, E. and Lueg, W., (1933), "Untersuchungen uber die Spannungsverteilung im Walzspalt," *Mitteilungen aus dem Kaiser Wilhelm Institut Eisenforschung*, Vol. 15, No. 1, pp 1-14.

Tieu A. K., You C., Zhu H. T., Lu C., Jiang Z. Y., and Giovanni D'Alessio, (2005), "Material Resistance and Friction in Cold Rolling," 6th World Congress of Structural and Multidisciplinary Optimization, Rio de Janeiro, 30th May – 3rd June 2005, Brazil.

Tieu, A. K. and Liu, Y. J., (2004), "Friction Variation in the Cold Rolling Process," *Tribology International*, Vol. 37, pp. 177-183.

Truncer, C. and Dean, T. A., (1987), "A New Pin Design for Pressure Measurements in Metal Forming Processes," *International Journal of Machine Tools Manufacturing*, Vol. 27, No. 3, pp. 325-331.

Yuen W.Y.D., Dixon A., Nguyen D.N., (1996), "The Modeling of the Mechanics of Deformation in Flat Rolling," *Journal of Materials Processing Technology*, Vol. 60, pp. 87-94.

Zhang S. and Lenard J. G., (1992), "The Effects of the Reduction, Speed and Lubricant Viscosity on Friction in Cold rolling," *Journal of Materials Processing Technology*, Vol. 30, pp. 197-209.

APPENDIX A

STRESS EQUATION DERIVATION

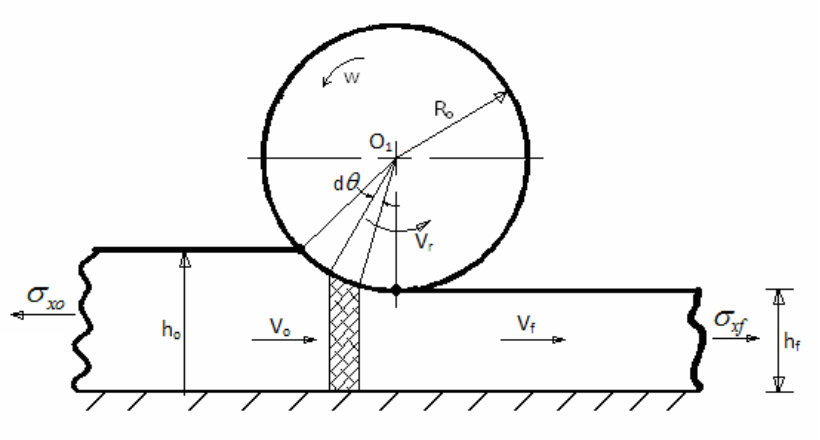

Figure A.1. Plastic Rolling Contact Model

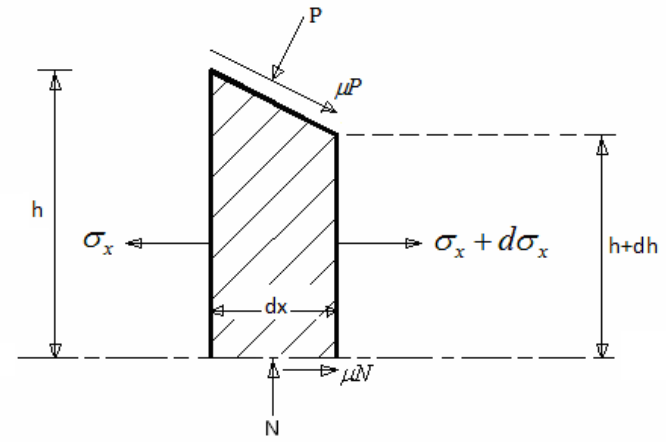

Figure A.2. Elemental Strip of Contact Model

The shearing stress is given by the relation $\tau = \mu P$. These stresses are resolved into their horizontal and vertical components. The stress σ_x is assumed to be uniformly distributed over the vertical faces of the element. The normal stress on one end of the element is $PR\,\partial\theta$, and the horizontal component of this force is $PR\sin\theta\partial\theta$. The tangential friction force is $\mu PR\partial\theta$, and its horizontal component is $\mu PR\cos\theta\partial\theta$. Summation of

the horizontal and vertical forces on the element (Figure A.2) results in stress equations in Equations A.1 and A2 respectively.

$$(\sigma_x + \partial\sigma_x)(h + \partial h) + \mu PR\cos\theta\partial\theta + \mu N - PR\sin\theta\partial\theta - \sigma_x h = 0 \tag{A.1}$$

$$\mu PR\sin\theta\partial\theta + PR\cos\theta\partial\theta - N = 0 \tag{A.2}$$

Further simplification of Equations A.1 and A.2 and eliminating small changes results in Equations A.3, A.4, A.5 and A.6.

$$\sigma_x h + h\partial\sigma_x + \partial\sigma_x h + \partial\sigma_x\partial h \pm \mu PR\cos\theta\partial\theta + \mu^2 PR\sin\theta\partial\theta + \mu PR\cos\theta\partial\theta - PR\sin\theta\partial\theta - \sigma_x h = 0 \tag{A.3}$$

$$\sigma_x\partial h + h\partial\sigma_x \pm \mu PR\cos\theta\partial\theta + \mu^2 PR\sin\theta\partial\theta + \mu PR\cos\theta\partial\theta - PR\sin\theta\partial\theta = 0 \tag{A.4}$$

$$\partial(\sigma_x h) + PR\left[\sin\theta(1+\mu) \pm \cos\left(\mu + \mu^2\right)\right]\partial\theta = 0 \tag{A.5}$$

$$\frac{\partial(\sigma_x h)}{\partial\theta} = P_\theta R\left[\sin\theta(1+\mu_\theta) \pm \cos\left(\mu_\theta + {\mu_\theta}^2\right)\right] \tag{A.6}$$

APPENDIX B

MATLAB PROGRAMS

Matlab Program 1

This program determines friction coefficient as a function of roll angle. The program uses Equation 3.7 and 3.10. The program input variables are draft (d), roll radius (R), initial thickness (h_o), and step size ($\Delta\theta$). The output is a function of friction coefficient with roll angle.

```
function Matlab_1
clear all
theta(1)=0;
R= input('specify the roll radius = '); %270;
draft=input('specify the draft variable' = '); %1.96;
d=draft/2;
thetamax=acos((R-d)/R);
sigma= input('specify the yield strength = ') %175;
L(1)=0;
h(1)= input('specify the exit thickness'); %25;
t(1)=sigma*h(1);
phi= input('specify the phi'); %1.2;
d_theta= input('specify the step size of theta'); %0.005;
XL=thetamax/d_theta;

Model= menu('choose scheme','Tieu Model',Avitzur Model')

if Model =1
Tieu Model
for i=1:XL
    theta(i+1)=theta(i)+d_theta;
    h(i+1)=h(i)+2*R*(1-cos(theta(i+1)));
    r(i+1)=(h(i+1)-h(i))/h(i+1);
```

```
    L(i+1)=L(i)*h(i)*phi/h(i+1);
    m(i)=0.086;
mu(i)=(0.01469+0.00298*h(i+1)+0.00167*r(i+1))*1.09979/(1+0.
000929*L(i+1));
end
sol=[mu]
th=theta(1:XL);
plot(th,mu,'r','lineWidth',3)
xlabel('Roll Angle - radians')
ylabel('Coefficient of Friction')
title('Modified Tieu Model')

elseif Model =2
Avitzur Model
for i=1:XL
    theta(i+1)=theta(i)+d_theta;
    h(i+1)=h(i)+2*R*(1-cos(theta(i+1)));
    t(i+1)=sigma*h(i+1);
    a(i)=h(i)/R;
    b(i)=h(i)/h(i+1);
    c(i)=t(i)-t(i+1);
    d=2*sigma/sqrt(3);
num(i)=0.5*a(i)^0.5.*(log(b(i))+((0.25*(a(i))^0.5*((1/b(i))
-1)^0.5+((-c(i))/d))));
den(i)=(((log(1/b(i))-1)*((c(i))/(d*(b(i)+1)^0.5)))-
(((1/d)*(t(i)-(c(i))/(b(i)-1))-1)*(atan(sqrt((1/b(i))-
1)))));
mu(i)=num(i)/den(i);
end
```

```
sol=[mu]
th=theta(1:XL);
plot(th,mu,'b','lineWidth',3)
xlabel('Roll Angle - radians')
ylabel('Coefficient of Friction')
title('Modified Avitzur Model')

else
disp('You did not choose the correct model')
end
```

Sample Input

R=270mm

d=1.96mm

h_o=25mm

$\Delta\theta$=0.005

Sample Output

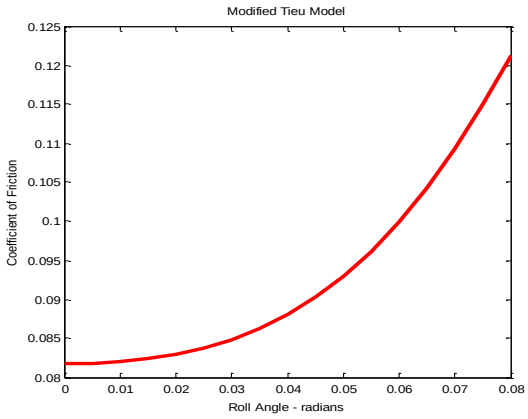

Matlab Program 2

This program identifies the location of "no slip" in the modified Tieu model. The program input is $\mu = f(\theta)$ derived from program 1. The output is given by θ_{NS}.

```
function Matlab_2
clear all
theta(1)=0;
R= input('specify the roll radius'); %270;
draft= input('specify the draft variable'); % 1.96;
d=draft/2
thetamax=acos((R-d)/R);
sigma= input('specify the yield strength); %175;
t(1)=sigma*h(1);
L(1)=0;
h(1)= input('specify the exit thickness');% 25;
phi= input('specify the phi');% 1.2;
d_theta= input('specify the delta_theta');% 0.005;
XL=thetamax/d_theta;
for i=1:XL
    theta(i+1)=theta(i)+d_theta;
    h(i+1)=h(i)+2*R*(1-cos(theta(i+1)));
    r(i+1)=(h(i+1)-h(i))/h(i+1);
    L(i+1)=L(i)*h(i)*phi/h(i+1);
    m(i)=0.086;

mu(i)=(0.01469+0.00298*h(i+1)+0.00167*r(i+1))*1.09979/(1+0.
000929*L(i+1));
mubefore(i)=10.11*(theta*theta)(i)-0.3877*theta(i)+0.0871;
muafter(i)=0.083;
```

```
     if mubefore=muafter
     theta(i)=thetans
else theta(i)=theta(i+1)
end

%Avitzur
for i=1:XL
    theta(i+1)=theta(i)+d_theta;
    h(i+1)=h(i)+2*R*(1-cos(theta(i+1)));
    t(i+1)=sigma*h(i+1);
    a(i)=h(i)/R;
    b(i)=h(i)/h(i+1);
    c(i)=t(i)-t(i+1);
    d=2*sigma/sqrt(3);
    num(i)=0.5*a(i)^0.5.*(log(b(i))+((0.25*(a(i))^0.5*((1/b
    (i))-1)^0.5+((-c(i))/d))));
    den(i)=(((log(1/b(i))-1)*((c(i))/(d*(b(i)+1)^0.5)))-
    (((1/d)*(t(i)-(c(i))/(b(i)-1))-1)*(atan(sqrt((1/b(i))-
    1)))));
    mu(i)=num(i)/den(i);
     mubefore(i)=0.8395*theta(i)+0.1002;
     muafter(i)=106*(theta*theta)(i)+0.3877*theta(i)+0.0508
     if mubefore=muafter
     theta(i)=thetans
     else theta(i)=theta(i+1)
end

%Measured
for i=1:XL
    theta(i+1)=theta(i)+d_theta;
```

```
muafter(i)=0.3077*theta(i)+0.0452;
mubefore(i)=-0.2105*(theta*theta)(i)+0.2087*theta(i)
+0.0606;
     if mubefore=muafter
     theta(i)=thetans
     else theta(i)=theta(i+1)
end
```

Sample Input

R= input('specify the roll radius');% 270mm

d= input('specify the draft'); %1.96mm

h_o= input('specify the exit thickness');%25mm

$\Delta\theta$= input('specify the delta_theta'); % 0.005

$\mu_{Before} = 10.11\theta^2 - 0.3877\theta + 0.0871$

$\mu_{After} = 0.083$

Sample Output

thetans = 0.0184

Matlab Program 3

This program estimates pressure distribution using constant friction coefficient model. The program uses Equations 1.6,1.7, 1.8, and 1.9. The input variables are draft (d), roll radius (R), initial thickness (h_o), yield strength (σ_y) and step size ($\Delta\theta$). The output is a pressure distribution pattern within the contact region.

```
function Matlab_6
clear all
draft= input('specify the …')1.96;
tf= input('specify the exit thickness')25;
to=tf+draft; %
R= input('specify the roll radius')270;
sigma= input('specify the yield strength');%175;
sigmab= input('specify the back tension');%0; %*to;
sigmaf= input('specify the front tension');%0; %*tf;
d=draft/2; %
thetae=acos((R-d)/R);
K=sigma/((3)^0.5);
t(1)= input('specify the …');%25;
theta(1)=0;
mu= input('specify the …');%0.1
lamdae=2*(R/tf)^0.5*atan(((R/tf)^0.5)*thetae);
lamdan=0.5*((1/mu)*log((tf/to)*((1-(sigb/2*K)/(1-
(sigf/2*K))))))+lamdae);
thetan=(tf/R)^0.5*tan((lamdan/2)*(tf/R)^0.5);
d_theta=0.1*thetan;
XL=(thetae/d_theta)+1;
lamda(1)=0;
for i=1:XL
```

```
        theta(i)=(i-1)*d_theta+theta(1);
        lamda(i)=2*(R/tf)^0.5*atan(((R/tf)^0.5)*theta(i));
        t(i)=t(1)+2*R*(1-cos(theta(i)));

        if theta<=thetan

              P(i)=2*K*(t(i)/tf)*(1-
              (sigmaf/(2*K)))*exp(mu*(lamda(i)));
              t1=theta;
              P1=P/(2*K);
              Q=P1;
        else
              P(i)=2*K*(t(i)/to)*(1-
              (sigmab/(2*K)))*exp(mu*(lamdae-lamda(i)));
              t2=theta((length(Q)):length(P));
              P1=P/(2*K);
              W=P1((length(Q)):length(P));
        end
              P1=P/(2*K);
end
plot(theta,P1,'lineWidth',3);
title('Pressure Distribution Rule of Thumb');
xlabel('Roll Angle - [radians]')
ylabel('P / 2 * K')
figure
plot(t1,Q);
q=polyfit(t1,Q,4);
f=q(1)*t1.^4+q(2)*t1.^3+q(3)*t1.^2+q(4)*t1+q(5);
y=@(t1) q(1)*t1.^4+q(2)*t1.^3+q(3)*t1.^2+q(4)*t1+q(5);
Area1=quadl(y,t1(1),thetan)
```

```
plot(t1,f)
figure
plot(t2,W);
p=polyfit(t2,W,4)
f1=p(1)*t2.^4+p(2)*t2.^3+p(3)*t2.^2+p(4)*t2+p(5);
y1=@(t2) p(1)*t2.^4+p(2)*t2.^3+p(3)*t2.^2+p(4)*t2+p(5);
plot(t2,f1)
Area2=quadl(y1,thetan,theta(length(t2)))
Area=Area1+Area2
```

Sample Input

R=270mm

d=1.96mm

h_o=25mm

$\Delta\theta$=0.005

σ_y=175N/mm^2

Sample Output

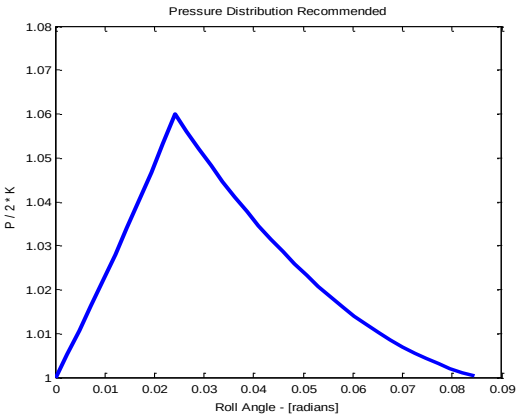

Matlab Program 4

This program estimates pressure distribution using varying friction coefficient model. The program uses Equations 3.8, 3.9, 3.11, 3.12, 4.1, 4.2, 4.12. The input variables are draft (d), roll radius (R), initial thickness (h_o), yield strength (σ_y) and step size ($\Delta\theta$). The output is a pressure distribution pattern within the contact region.

```
function Matlab_4
clear all
draft= input('specify the draft');%1.96;
d=draft/2;
tf= input('specify the exit thickness');%25;
to=tf+draft;
r=1-(tf/to);
R= input('specify the roll radius');%270;
thetae=acos((R-d)/R);
L=10000;
sigma= input('specify the yield strength');%175;
K=sigma/((3)^0.5);
d_theta=0.1*thetan;
XL=(thetae/d_theta)+1;
%Avitzur Model
mu1=0.5*(tf/R)^0.5*(log(to/tf)+0.25*(tf/to)^0.5.*((to/tf)-
1)^0.5+(sigb-sigf)/((2/(3)^0.5)*sigma));
mu2=((log((to/tf)-1)*((sigf-
sigb)/((2/(3)^0.5)*sigma*(((to/tf)-1)^0.5)))));
mu3=(1/((2/((3)^0.5)*sigma))*(sigb-((sigf-sigb)/((to/tf)-
1)))-1)*atan(sqrt((to/tf)-1));
mu=mu1/(mu2-mu3);
```

```
%Tieu Model
     h(i+1)=h(1)+2*R*(1-cos(theta(i+1)));
     r(i+1)=(h(i+1)-h(1))/h(1);
     L(i+1)=L(i)*h(i)*phi/h(i+1);
     mu(i+1)=(0.01469+0.00298*h(i+1)+0.00167*r(i+1))*1.0997
     9/(1+0.000929*L(i+1));
for i=1:XL

     if theta<=thetan
     P(i+1)=((2*P(i)*R*e(i)*f1(i)*d_theta+g(i)*P(i)*e(i)+2*
     h(i)*P(i)*P(i)*(-mu(i))*m(i)-2*g(i)*e1(i))/-
     (h(i)*e(i)+2*h(i)*P(i)*mu(i)*mu(i)))+P(i);
          t1=theta;
          P1=P/(2*K);
          Q=P1;
     else
     P(i+1)=((2*P(i)*R*e(i)*f(i)*d_theta+g(i)*P(i)*e(i)+2*h
     (i)*P(i)*P(i)*P(i)*P(i)*mu(i)*m(i)-2*g(i)*e1(i))/-
     (h(i)*e(i)+2*h(i)*P(i)*mu(i)*mu(i)))+P(i);
          P1=P/(2*K);
          W=P1((length(Q)):length(P));
     end
end
plot(theta,P1,'k','lineWidth',3);
title('Pressure Distribution Measured')
xlabel('Roll Angle - [radians]')
ylabel('P / 2 * K')
figure
plot(t1,Q);
q=polyfit(t1,Q,4);
```

```
f=q(1)*t1.^4+q(2)*t1.^3+q(3)*t1.^2+q(4)*t1+q(5);%
y=@(t1) q(1)*t1.^4+q(2)*t1.^3+q(3)*t1.^2+q(4)*t1+q(5);
Area1=quadl(y,t1(1),thetan)
plot(t1,f)
figure
plot(t2,W);
p=polyfit(t2,W,4)
f1=p(1)*t2.^4+p(2)*t2.^3+p(3)*t2.^2+p(4)*t2+p(5);
y1=@(t2) p(1)*t2.^4+p(2)*t2.^3+p(3)*t2.^2+p(4)*t2+p(5);
plot(t2,f1)
Area2=quadl(y1,thetan,theta(length(t2)))
Area=Area1+Area2
```

Sample Input

R=270mm

d=1.96mm

h_o=25mm

$\Delta\theta$=0.005

σ_y=175N/mm^2

Sample Output

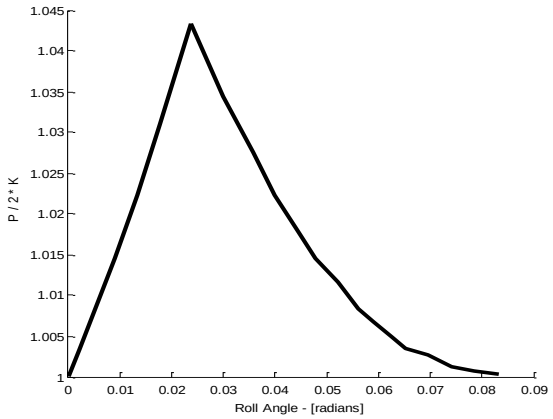

Matlab Program 5

This program estimates pressure distribution with strain hardening effects using the varying friction coefficient model. The program used Equations 3.8, 3.9, 3.11, 3.12, 4.1, 4.2 and 4.17. The input variables are draft (d), roll radius (R), initial thickness (h_o), yield strength (σ_y) and step size ($\Delta\theta$). The output is a pressure distribution pattern within the contact region

```
function Matlab_10
clear all
theta(1)=0;
h(1)= input('specify the exit thickness');%25;
draft= input('specify the draft');%1.96;
d=draft/2;
R= input('specify the roll radius');%270;
thetamax=acos((R-d)/R);
sigma= input('specify the yield strength');%175;
thetan= input('specify the no-slip point');%0.022;
d_theta=0.1*thetan;
XL=(thetamax/d_theta)+1;
%Modified Tieu
h(i+1)=h(1)+2*R*(1-cos(theta(i+1)));
r(i+1)=(h(i+1)-h(1))/h(1);
L(i+1)=L(i)*h(i)*phi/h(i+1);
mu(i+1)=(0.01469+0.00298*h(i+1)+0.00167*r(i+1))*1.09979/(1+
0.000929*L(i+1));

for i=1:XL
    theta(i)=theta(1)+i*d_theta;
     theta(i+1)=theta(1)+i*d_theta;
```

```
 h(i+1)=h(1)+2*R*(1-cos(theta(i+1)));
 t(i+1)=sigma*h(i+1);
 a(i)=h(i)/R;
 b(i)=h(i)/h(i+1);
 c(i)=t(i)-t(i+1);
 d=2*sigma/sqrt(3);
 num(i)=0.5*a(i)^0.5.*(log(b(i))+((0.25*(a(i))^0.5*((1/
 b(i))-1)^0.5+((-c(i))/d))));
den(i)=(((log(1/b(i))-1)*((c(i))/(d*(b(i)+1)^0.5)))-
(((1/d)*(t(i)-(c(i))/(b(i)-1))-1)*(atan(sqrt((1/b(i))-
1)))));
 mu(i+1)=num(i)/den(i);
 e(i)=sqrt((d/2)^2-(P(i)*mu(i))^2);
 e1(i)=((d/2)^2-(P(i)*mu(i))^2);
 f(i)=(sin(theta(i))+mu(i)*cos(theta(i)));
 f1(i)=(sin(theta(i))-mu(i)*cos(theta(i)));% minus
 g(i)=(h(i+1)-h(i));
 m(i)=(mu(i+1)-mu(i));
if theta <= thetan
  t1=theta;
 P(i+1)=((2*P(i)*R*e(i)*f1(i)*d_theta+g(i)*P(i)*e(i)+2*
 h(i)*P(i)*P(i)*(-mu(i))*m(i)-2*g(i)*e1(i))/-
 (h(i)*e(i)+2*h(i)*P(i)*mu(i)*mu(i)))+P(i);
      Q=P;
else
 P(i+1)=((2*P(i)*R*e(i)*f(i)*d_theta+g(i)*P(i)*e(i)+2*h
 (i)*P(i)*P(i)*mu(i)*m(i)-2*g(i)*e1(i))/-
 (h(i)*e(i)+2*h(i)*P(i)*mu(i)*mu(i)))+P(i);
      t2=theta((length(Q)):length(P));
 W=P((length(Q)):length(P));
```

```
    end
end
plot(theta,P,'c','LineWidth',3);
xlabel('Roll Angle - [radians]')
ylabel('P / 2 * K')
```

Sample Input

R=270mm

d=1.96mm

h_o=25mm

$\Delta\theta$=0.005

σ_y=175N/mm^2

Sample Output

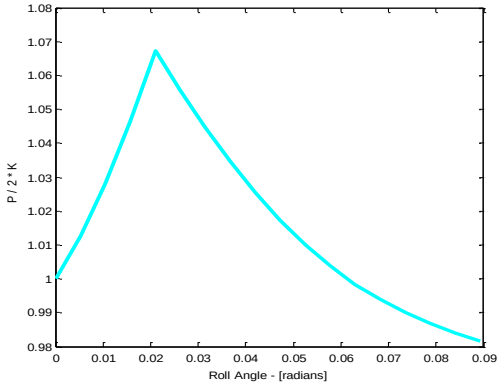

APPENDIX C

DESIGN FEATURES OF SGROLL

APPENDIX D

CALIBRATION OF TANGENTIAL AND RADIAL SENSING ELEMENTS

Figure D1. Photograph of Experimental Set Up for Strain Gauge Calibration

Figure D2. Details of Strain Gauge and Fixture

Figure D3. Data Acquisition System

Table D1. Results of Radial Strain Calibration

Force (Ibf)	Strain (micro-in/in)				
	1	**2**	**3**	**4**	**Average**
0	0	0	0	0	0
3	63	63	63	63	63
13	291	291	291	291	291
23	519	518	519	518	519
33	749	750	749	750	750
43	983	982	982	982	982
53	1213	1217	1214	1217	1215

Table D2. Results of Tangential Strain Calibration

Force (Ibf)	Strain (micro-in/in)				
	1	**2**	**3**	**4**	**Average**
0	0	0	0	0	0
3	26	26	27	27	27
13	121	120	120	120	120
23	214	214	214	215	214
33	310	311	311	310	311
43	409	409	409	409	409
53	511	511	511	510	511

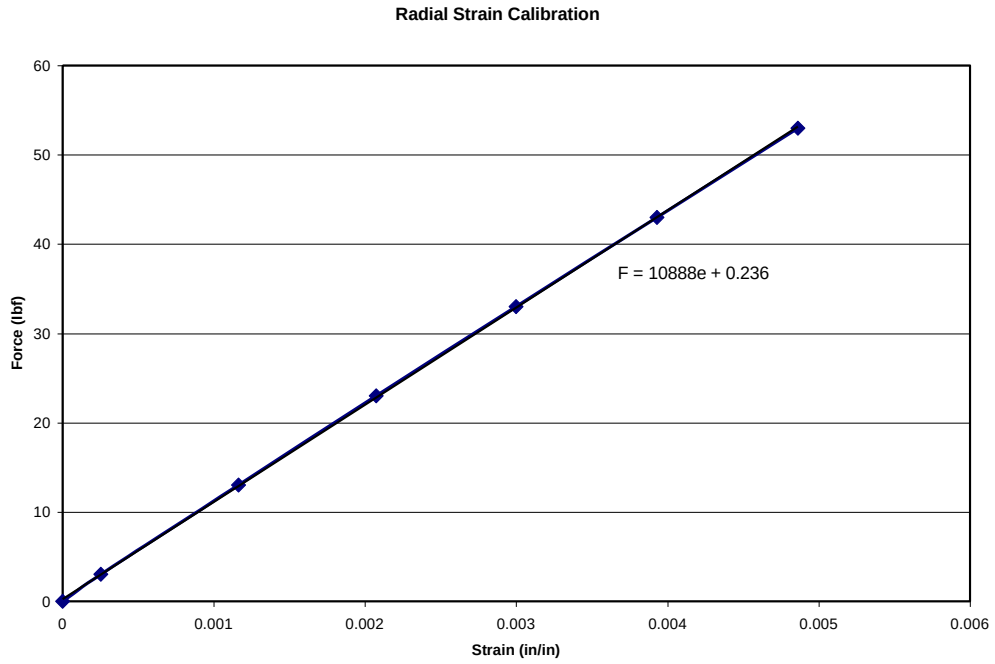

Figure D4. Graph of Radial Strain Calibration

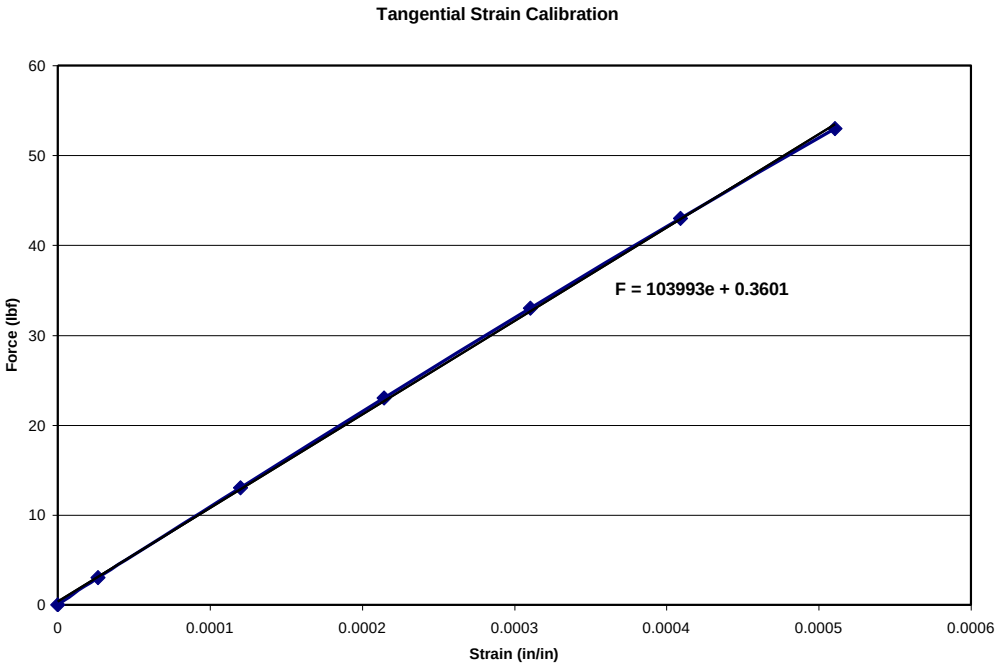

Figure D5. Graph of Tangential Strain Calibration

APPENDIX E

SELECTION OF ROLLING PARAMETERS

Rolling Mill Parameters

Roll Radius R_0 = 1 inch

Speed Range $= 0$ *to* $20\,rev/\min$

Entry Thickness $h_0 = 0.375 inch$

Exit Thickness $h_1 = h_0(1-r)$, $d = h_0 - h_1 = rh_0$, *Where r = reduction ratio*

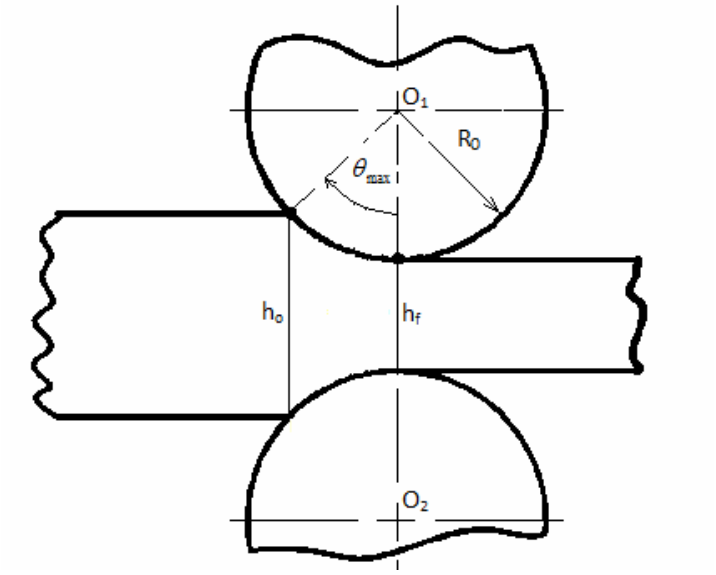

Now from geometry, $\theta_{\max} = \cos^{-1}\left(\frac{2R_0 - rh_0}{2R_0}\right)$, *time*, $t = \frac{\theta_{\max}}{2\pi N}$. Choose *N=5rev/min*.

For *r=10%*, θ_{max}*= 0.194 radians, and t = 0.37secs*

For *r=20%*, θ_{max}*= 0.275 radians, and t = 0.525secs*

For *r=30%*, θ_{max}*= 0.337 radians, and t = 0.644secs*

Data Acquisition Parameters

Maximum Sampling Rate 100 Hz. Data is sampled for every 0.01 seconds

From the above analysis, choose r = 30%. Choice of speed and aging in rolling equipment cannot roll higher reduction ratio at one pass. With r = 30% : 64 data points.

APPENDIX F

DATA AND ANALYSIS OF THE ROLLING EXPERIMENT

Table F1. Raw Data of Rolling Experiment – r = 30%, N = 5 rev/min

Time (s)	Strain (micro - in/in)	
	Channel 1 (Radial)	Channel 2 (Tangential)
0.00	42438	469
0.01	42539	468
0.02	42640	468
0.03	42833	468
0.04	42842	465
0.05	42943	462
0.06	43044	458
0.07	43145	455
0.08	43246	452
0.09	43347	448
0.10	43448	445
0.11	43549	442
0.12	43650	439
0.13	43751	435
0.14	43852	432
0.15	43953	429
0.16	44054	426
0.17	44155	422
0.18	44256	419
0.19	44357	416
0.20	44458	413
0.21	44560	409
0.22	44633	406
0.23	44670	403
0.24	44706	399
0.25	44743	396
0.26	44780	393
0.27	44817	390
0.28	44853	386
0.29	44890	383
0.30	44927	380
0.31	44964	377
0.32	45000	373
0.33	45037	370
0.34	45074	367
0.35	45111	363
0.36	45147	365
0.37	45184	366

Table F1 Cont. Raw Data of Rolling Experiment – r = 30%, N = 5 rev/min

Time (s)	Strain (micro - in/in)	
	Channel 1 (Radial)	Channel 2 (Tangential)
0.38	45221	367
0.39	45258	368
0.40	45294	369
0.41	45331	370
0.42	45368	371
0.43	45404	372
0.44	45441	373
0.45	45349	364
0.46	45184	356
0.47	45019	347
0.48	44853	339
0.49	44688	331
0.50	44523	323
0.51	44357	315
0.52	44192	307
0.53	44027	298
0.54	43861	290
0.55	43696	282
0.56	43531	274
0.57	43366	266
0.58	43200	258
0.59	43035	249
0.60	42870	241
0.61	42704	233
0.62	42539	225
0.63	42374	217
0.64	42208	208
0.65	42043	200

Table F2. Analysis of Rolling Experiment – r = 30%, N = 5 rev/min

Time (s)	θ (rad)	Strain - Force Calibration		μ
		Normal Force (lbf)	Friction Force (lbf)	
0	0.337	462	49	0.1062
0.01	0.332	463	49	0.1059
0.02	0.327	465	49	0.1056
0.03	0.321	467	49	0.1051
0.04	0.316	467	49	0.1043
0.05	0.311	468	48	0.1034
0.06	0.306	469	48	0.1024
0.07	0.301	470	48	0.1014
0.08	0.295	471	47	0.1005
0.09	0.290	472	47	0.0995
0.10	0.285	473	47	0.0986
0.11	0.280	474	46	0.0976
0.12	0.275	476	46	0.0967
0.13	0.269	477	46	0.0958
0.14	0.264	478	45	0.0948
0.15	0.259	479	45	0.0939
0.16	0.254	480	45	0.0930
0.17	0.249	481	44	0.0921
0.18	0.243	482	44	0.0911
0.19	0.238	483	44	0.0902
0.20	0.233	484	43	0.0893
0.21	0.228	485	43	0.0884
0.22	0.223	486	43	0.0876
0.23	0.217	487	42	0.0868
0.24	0.212	487	42	0.0860
0.25	0.207	487	42	0.0853
0.26	0.202	488	41	0.0845
0.27	0.197	488	41	0.0837
0.28	0.191	489	41	0.0830
0.29	0.186	489	40	0.0822
0.30	0.181	489	40	0.0814
0.31	0.176	490	40	0.0807
0.32	0.171	490	39	0.0799
0.33	0.165	491	39	0.0792
0.34	0.160	491	39	0.0784
0.35	0.155	491	38	0.0777
0.36	0.150	492	38	0.0778

Table F2 Cont. Analysis of Rolling Experiment – r = 30%, N = 5 rev/min

Time (s)	θ (rad)	Strain - Force Calibration		μ
		Normal Force (lbf)	Friction Force (lbf)	
0.37	0.145	492	38	0.0780
0.38	0.139	493	38	0.0781
0.39	0.134	493	39	0.0783
0.40	0.129	493	39	0.0785
0.41	0.124	494	39	0.0786
0.42	0.119	494	39	0.0788
0.43	0.113	495	39	0.0789
0.44	0.108	495	39	0.0791
0.45	0.103	494	38	0.0773
0.46	0.098	492	37	0.0759
0.47	0.093	490	36	0.0744
0.48	0.087	489	36	0.0729
0.49	0.082	487	35	0.0715
0.50	0.077	485	34	0.0700
0.51	0.072	483	33	0.0685
0.52	0.067	481	32	0.0670
0.53	0.061	480	31	0.0655
0.54	0.056	478	31	0.0639
0.55	0.051	476	30	0.0624
0.56	0.046	474	29	0.0608
0.57	0.041	472	28	0.0593
0.58	0.035	471	27	0.0577
0.59	0.030	469	26	0.0561
0.60	0.025	467	25	0.0545
0.61	0.020	465	25	0.0529
0.62	0.015	463	24	0.0512
0.63	0.009	462	23	0.0496
0.64	0.004	460	22	0.0479
0.65	0.000	458	21	0.0463